0830-L-02 NAS 1.29/3-2:98-11

NASA TechBriefs

National Aeronautics and
Space Administration

Electronic Components and Circuits

Electronic Systems

Physical Sciences

CONTROL

Materials

Computer Programs

Mechanics

Machinery

Fabrication Technology

Mathematics and Information Sciences

Life Sciences

98-11

November 1998

for 99-007628

COMPLETED

no

INTRODUCTION

Tech Briefs are short announcements of new technology derived from the research and development activities of the National Aeronautics and Space Administration. These Briefs emphasize information considered likely to be transferable across industrial, regional, or disciplinary lines and are issued to encourage commercial application.

Availability of NASA Tech Briefs and TSP's

Distribution of NASA Tech Briefs, a monthly periodical publication, is limited to engineers in U.S. industry and to other domestic technology transfer agents. Requests for individual Tech Briefs or for Technical Support Packages (TSP's) announced herein should be addressed to

NASA Center for AeroSpace Information
Technology Transfer Office
800 Elkridge Landing Rd.
Linthicum Heights, MD 21090-2934
Telephone No. (301) 621-0245

Please reference the three-letter, five-digit control number located at the end of each Tech Brief. Information on NASA's Technology Utilization Program, its documents, and services is also available at the same facility.

Technology Utilization Officers and Patent Counsels are located at NASA field installations to provide technology-transfer access to industrial users. Inquiries can be made by writing to NASA field installations listed below.

Technology Utilization Officers and Patent Counsels

Ames Research Center
Technology Utilization Officer
Mail Code 223-3
Moffett Field, CA 94035

Patent Counsel
Mail Code 200-11
Moffett Field, CA 94035

Goddard Space Flight Center
Technology Utilization Officer
Mail Code 702-1
Greenbelt, MD 20771

Patent Counsel
Mail Code 204
Greenbelt, MD 20771

Lyndon B. Johnson Space Center
Technology Utilization Officer
Mail Code IC-4
Houston, TX 77058

Patent Counsel
Mail Code AL3
Houston, TX 77058

John F. Kennedy Space Center
Technology Utilization Officer
Mail Stop PT-PMO-A
Kennedy Space Center, FL 32899

Patent Counsel
Mail Code PT-PAT
Kennedy Space Center, FL 32899

Langley Research Center
Technology Utilization Officer
Mail Stop 143
Hampton, VA 23665

Patent Counsel
Mail Code 279
Hampton, VA 23665

Lewis Research Center
Technology Utilization Officer
Mail Stop 7-3
21000 Brookpark Road
Cleveland, OH 44135

Patent Counsel
Mail Code LE-LAW
21000 Brookpark Road
Cleveland, OH 44135

Jet Propulsion Laboratory
Technology Utilization Officer
Mail Stop 156-211
4800 Oak Grove Drive
Pasadena, CA 91109

NASA Resident Office-JPL
Technology Utilization Officer
Mail Stop 180-801
4800 Oak Grove Drive
Pasadena, CA 91109

Patent Counsel
Mail Code 180-801
4800 Oak Grove Drive
Pasadena, CA 91109

George C. Marshall Space Flight Center
Technology Utilization Officer
Code AT01
Marshall Space Flight Center, AL 35812

Patent Counsel
Mail Code CC01
Marshall Space Flight Center, AL 35812

John C. Stennis Space Center
Technology Utilization Officer
Code HA-30
Stennis Space Center, MS 39529

NASA Headquarters
Technology Utilization Officer
Code CU
Washington, DC 20546

Assistant General Counsel for Patent Matters
Code GP
Washington, DC 20546

Dryden Flight Research Center
Technology Utilization Officer
M/S D21-31
Bldg. 4832 Whse 7
Lilly Dr.
Edwards, CA 93523

BLANK PAGE

NASA TechBriefs

National Aeronautics and
Space Administration

November 1998
98-11

5 Electronic Components and Circuits

13 Electronic Systems

19 Physical Sciences

25 Materials

29 Computer Programs

33 Mechanics

41 Machinery

This document was prepared under the sponsorship of the National Aeronautics and Space Administration. Neither the United States Government nor any person acting on behalf of the United States Government assumes any liability resulting from the use of the information contained in this document, or warrants that such use will be free from privately owned rights.

BLANK PAGE

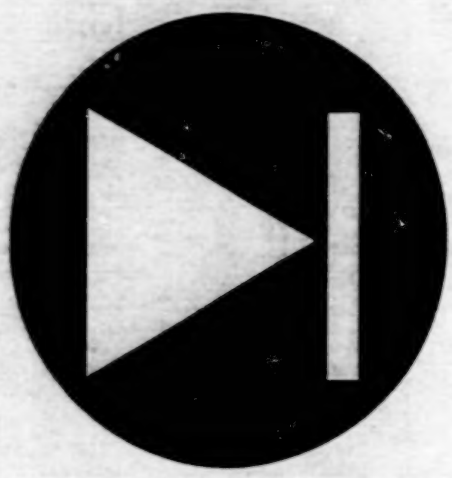

Electronic Components and Circuits

Hardware, Techniques, and Processes

7 Improved Electron-Tunneling Magnetometer
8 Apparatus for Measuring a Weak Induced Magnetic Field
9 Improved Tuning of a Microwave Cavity for Heating Samples
10 First-Generation "Space Cube" Electronic-Circuit Packaging
11 Micromachined Photodiode/Bolometer Arrays

BLANK PAGE

Improved Electron-Tunneling Magnetometer

A "planarized" design provides for improvements in fabrication and performance.

NASA's Jet Propulsion Laboratory, Pasadena, California

Efforts are underway to develop an electron-tunneling magnetometer with a "planarized" (as explained below) design. Older designs of electron-tunneling magnetometers are more three-dimensional in character and, as such, entail some difficulties of fabrication. [Such an older design was described in "Electron-Tunneling Magnetometer" (NPO-18493) *NASA Tech Briefs*, Vol. 17, No. 9 (September 1993), page 32.] Relative to the older designs, the present design offers advantages of sensitivity, manufacturability, and cost.

Like other tunneling-based microelectromechanical sensors, the developmental electron-tunneling magnetometer includes an electron-tunneling force/displacement transducer, wherein electrostatic-force feedback is used to counteract a force applied to a flexible cantilever or membrane by the phenomenon that one seeks to measure. The objective in the feedback scheme in any such sensor is to maintain, as close as possible to a prescribed value, the small distance between (a) a stationary tunneling tip and (b) a counterelectrode on the cantilever or membrane. The electrostatic-deflection voltage applied to maintain the prescribed gap bears a known proportionality to the force applied to the transducer by the phenomenon that one seeks to measure. In the case of an electron-tunneling magnetometer, one seeks to measure a magnetic field through the Lorentz force that the field exerts on a known electric current in a coil of wire attached to the cantilever or membrane.

A typical electron-tunneling magnetometer of older design is fabricated from two silicon wafers. One wafer is bulk-micromachined to form the tunneling tip in a base structure; the other wafer is bulk-micromachined to form a membrane about 0.5 μm thick, at the bottom of a well about 200 μm deep (see Figure 1). The wafers are then manually assembled (membrane wafer on top, tunneling-tip wafer below) and bonded together with epoxy. The difficulties associated with the older design arise principally in connection with fabrication of the coil of wire on the relatively thin membrane at the bottom of the relatively deep well. The fabrication difficulties lead to defects and thus to poor device yield and increased costs. In addition, the membrane-in-a-well configuration limits the achievable sensitivity.

In the present version, the design and

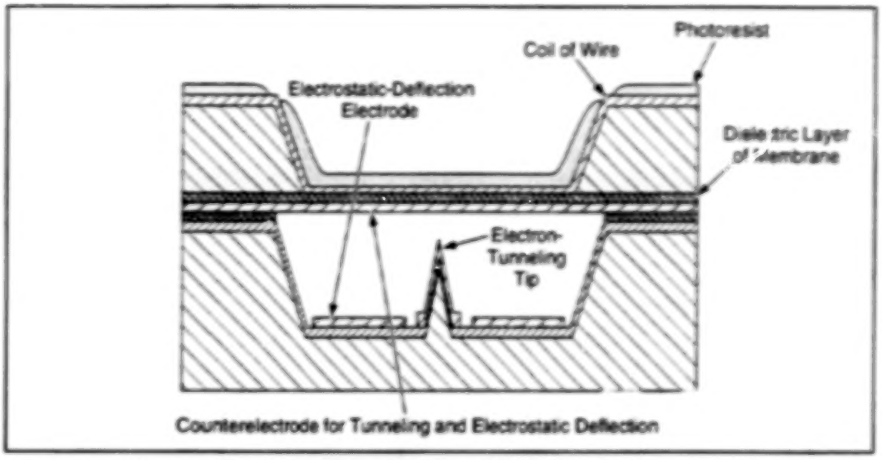

Figure 1. An **Electron-Tunneling Magnetometer of Older Design** is depicted here in a composite view of different stages of fabrication. Limitations on coil-line width arise from fabrication into the deep well.

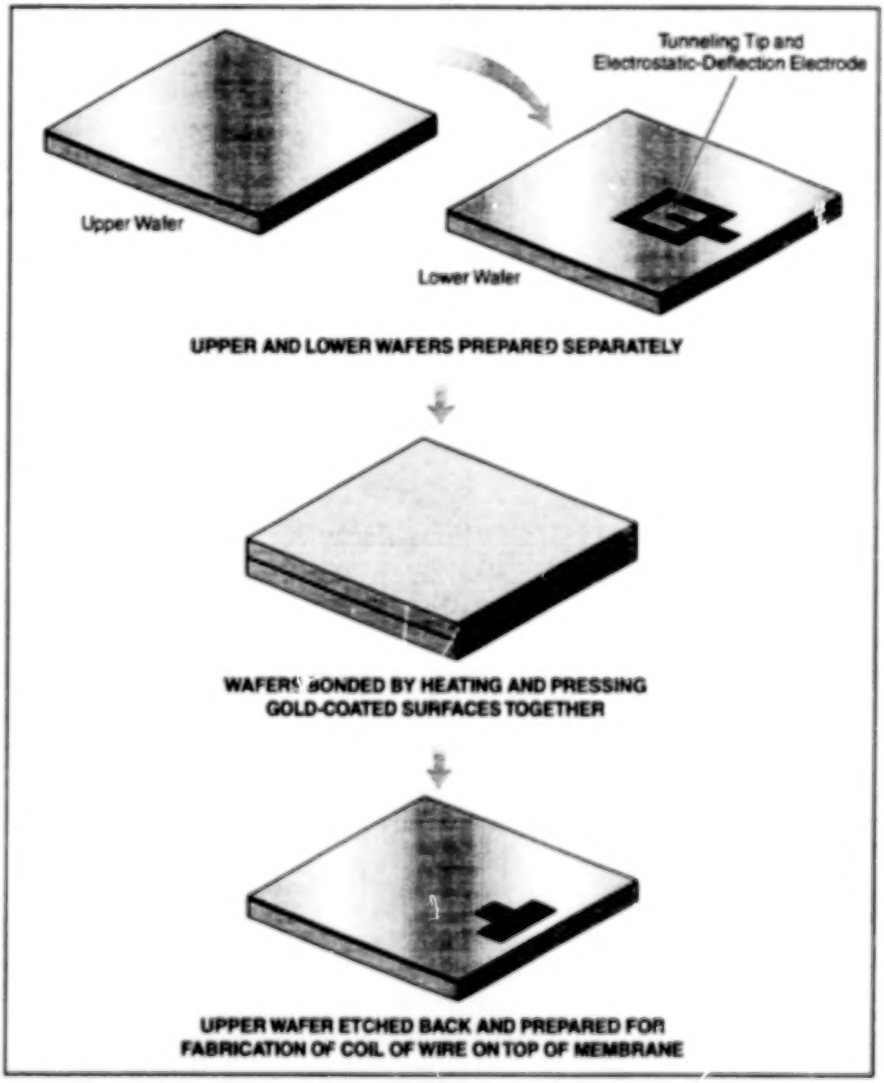
Tunneling Tip and Electrostatic-Deflection Electrode
Upper Wafer
Lower Wafer
UPPER AND LOWER WAFERS PREPARED SEPARATELY
WAFERS BONDED BY HEATING AND PRESSING GOLD-COATED SURFACES TOGETHER
UPPER WAFER ETCHED BACK AND PREPARED FOR FABRICATION OF COIL OF WIRE ON TOP OF MEMBRANE

Figure 2. In the **Newer "Planarized" Design**, there is no well, and the fabrication of the coil of wire on the upper surface of the membrane is deferred until after bonding of the two wafers and etch-back of the upper wafer to the required membrane thickness.

fabrication of the lower wafer are substantially the same as in the older design. However, the design of the upper wafer is different, the method of bonding the wafers is different, and most of the fabrication of the membrane in the upper wafer is deferred until after the wafers have been bonded together (see Figure 2). Prior to bonding, the faying surfaces of the two wafers (the lower surface of the upper wafer and the upper surface of the lower wafer) are coated with gold. The gold coat on the lower surface of the upper wafer is destined to become the electrode layer on the membrane; a window is formed in this coat to facilitate subsequent electrical contact with the tunneling tip and the lower electrostatic-deflection electrode.

The coated wafers are aligned, then bonded using a metal/metal thermocompression technique. Unlike in the older design, the membrane is not formed at the bottom of a well in the upper wafer. Instead, the entire upper surface of the upper wafer is etched back toward the gold layer to form the membrane, leaving a planar upper surface. Therefore, unlike in the older design, it is not necessary to manually align a recessed membrane on an upper wafer with a tunneling electrode on a lower wafer; as a result, manufacturability is enhanced and the cost of manufacture reduced. A fine coil of wire can be fabricated on top of the planar upper surface by use of conventional photoresist spin processing, more easily and with higher yield than in the case of a recessed membrane. The cost of manufacture is thus reduced further.

By enhancing manufacturability, yield, and robustness, the planarized design offers additional margin for optimization of design to increase sensitivity. As a result, noise-floor is projected to reach 10 $nT/Hz^{1/2}$, as compared with about 7 $\mu T/Hz^{1/2}$ in the older design.

This work was done by Linda Miller, Judith Podosek, and Indrani Chakraborty of Caltech for **NASA's Jet Propulsion Laboratory**. *Further information is contained in a TSP [see page 1].*

In accordance with Public Law 96-517, the contractor has elected to retain title to this invention. Inquiries concerning rights for its commercial use should be addressed to

Technology Reporting Office
JPL
Mail Stop 122-116
4800 Oak Grove Drive
Pasadena, CA 91109
(818) 354-2240

Refer to NPO-20317, volume and number of this NASA Tech Briefs *issue, and the page number.*

Apparatus for Measuring a Weak Induced Magnetic Field

A sensing coil lies in a magnetic cavity of two primary coils.

Stennis Space Center, Mississippi

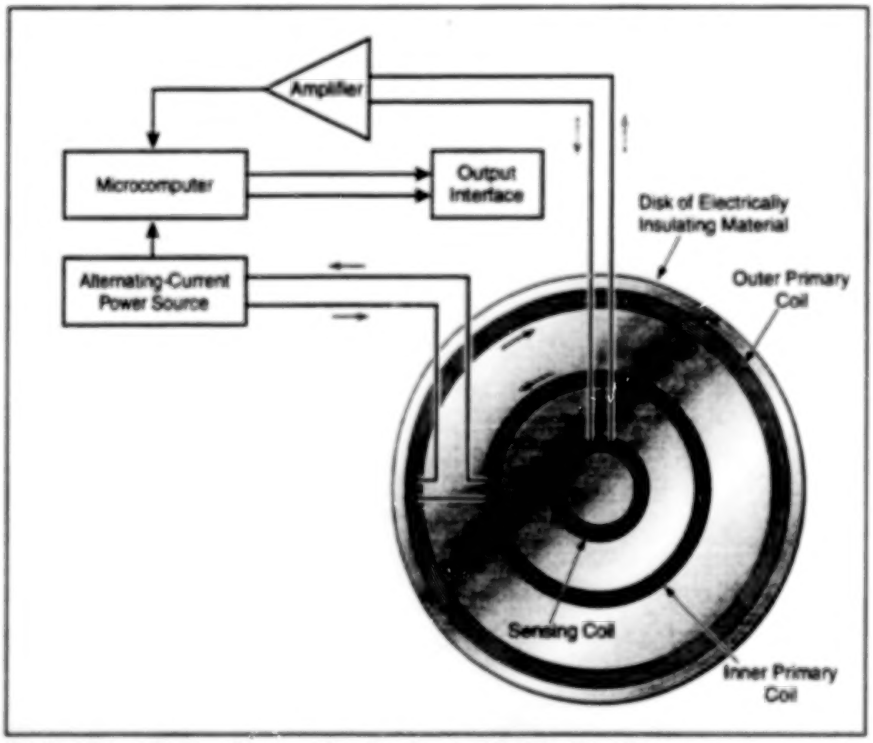

The Net Magnetic Flux Generated in the Sensing Coil by the primary coils can be made zero by suitable choice of the radius of the sensing coil and the radii and numbers of turns of the primary coils.

The figure illustrates an apparatus for inducing an electric current in an electrically conductive object or layer of material and measuring the magnetic field generated by the current (that is, the induced magnetic field) to obtain information about the object or layer. The apparatus can be used, for example, to detect metal objects buried underground.

Like older apparatuses developed for the same purpose, this apparatus includes (1) a primary electromagnet coil excited by alternating current to generate an excitatory alternating magnetic field in the object or layer of interest and (2) a sensing electromagnet coil to measure the induced magnetic field. Heretofore, it has been common practice to mount the primary coil as far a possible from the sensing coil to prevent the excitatory magnetic field from overwhelming the relatively weak induced magnetic field at the sensing coil; unavoidably, this results in a large apparatus. The present apparatus is more compact because the primary and sensing coils are mounted close to each other; indeed, they are mounted concentrically. Despite the proximity of the coils to each other, the excitatory magnetic field does not overwhelm the weak induced magnetic field at the sensing coil; on the contrary, as explained below, the coils are designed so that the net excitatory magnetic flux through the sensing coil is zero.

More precisely, there are two primary coils: a larger (outer) and a smaller (inner) one. The sensing coil is the smallest coil and lies within the inner primary coil. All three coils are mounted in a disk of polycarbonate or some other suitable electrically nonconductive material. The outer and inner primary coils are connected electrically in series, at opposite polarity, to a low-impedance ac power source. Thus, when power is applied, the two primary coils generate alternat-

ing magnetic fields of opposite polarity.

The magnetic fields generated by both primary coils at typical measurement distances (much greater than the diameter of the outer primary coil) are given by the well-known dipole approximation. In a typical design, the magnetic dipole moment of the outer primary coil is much greater than that of the inner primary coil, so that at typical measurement distances, the net excitatory magnetic field is dominated by the portion generated by the outer primary coil. However, near the center, where the sensing coil lies, the opposing magnetic fields from the two primary coils can be made approximately equal in magnitude, so that the net excitatory magnetic field can be made zero or nearly so within the sensing coil — in effect, placing the sensing coil in a magnetic cavity. By suitable choice of the numbers of turns and the radii of the inner and outer primary coils and the radius of the sensing coil according to established equations of electromagnetism, one can achieve a balance between the opposing excitatory fluxes intercepted by the sensing coil, so that the net excitatory flux through the sensing coil is zero.

In operation, a replica of the ac excitation is digitized and sent to a microcomputer. The electromagnetic force generated in the sensing coil by the induced magnetic field is amplified, then also digitized and sent to the microcomputer. In the microcomputer, the amplitude and phase of the signal from the sensing coil are compared with those of the ac excitation. The relative-amplitude and relative-phase information is displayed on an output interface. This information can be interpreted in terms of properties of the object or material to which the excitatory magnetic field has been applied.

This work was done by I. J. Won of Geophex Ltd. for **Stennis Space Center**.

In accordance with Public Law 96-517, the contractor has elected to retain title to this invention. Inquiries concerning rights for its commercial use should be addressed to

I. J. Won, PhD
Geophex, Ltd.
605 Mercury Street
Raleigh, NC 27603-2343
(919) 839-8515
e-mail: ijwon@geophex.com

Refer to SSC-00074, volume and number of this NASA Tech Briefs *issue, and the page number.*

Improved Tuning of a Microwave Cavity for Heating Samples

This technique is applicable to both z-dependent and z-independent modes.

NASA's Jet Propulsion Laboratory, Pasadena, California

A technique for adjusting the resonance frequency of a single-mode round cylindrical microwave cavity has been proposed to maximize the transfer of power from a magnetron to one or more sample(s) of material that have been placed in the cavity for microwave heating. Unlike an older technique that involves insertion of a dielectric stub into the cavity from an off-axis position, the proposed technique would preserve the desired angular symmetry of the electromagnetic mode. Unlike another older technique that involves moving a plunger along the cylindrical (*z*) axis, the proposed technique would be applicable to *z*-independent as well as to *z*-dependent modes.

For maximum transfer of power, the resonance frequency of the cavity must be maintained within the fixed frequency band (typically 5 to 15 MHz wide) of the magnetron. The need for tuning arises because the samples exert a detuning effect: they alter the resonance frequency by an amount that increases with the real part of the permittivity of the sample material. In general, insertion of samples causes the resonance frequency to decrease from the empty-cavity value. Moreover, the permittivities of most materials vary with temperature; in a typical case, the real part of the permittivity increases with temperature, leading to a further lowering of the resonance frequency during microwave heating.

The proposed technique would exploit the detuning effect of dielectric objects. Provision would be made for adjustable insertion of one or more concentric dielectric tuning object(s) (described below). The cavity would be constructed with a radius slightly less than the value needed to match the resonance of the magnetron in the empty-cavity condition; thus, prior to

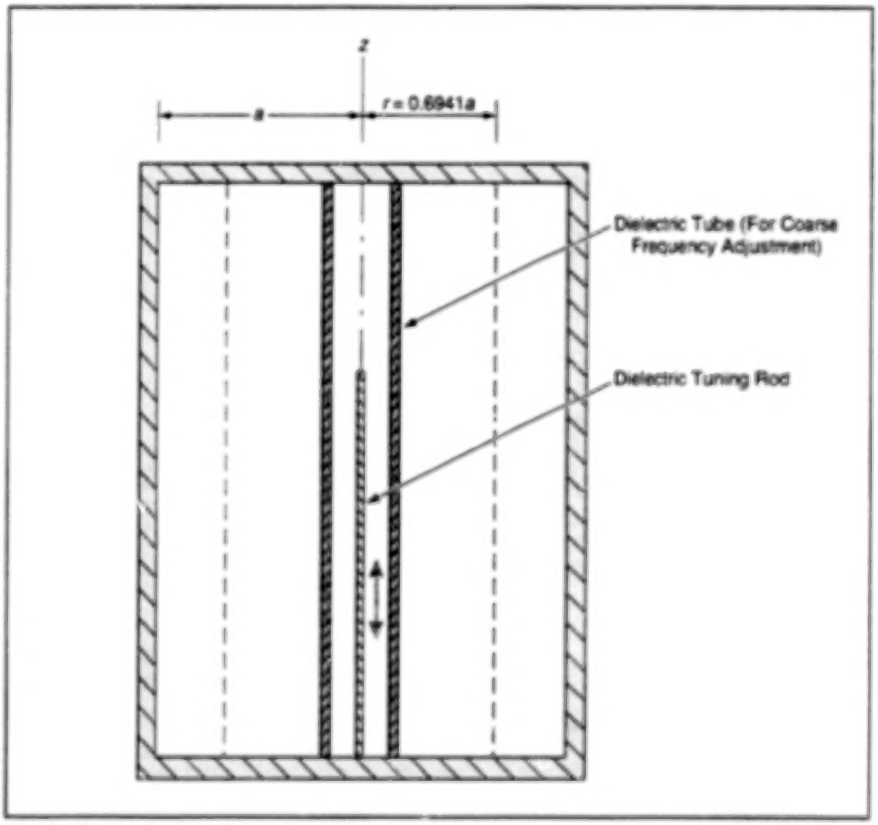

The Dielectric Rod and Tube would lower the resonance frequency of the cavity, which would have a resonance frequency slightly higher than the desired value when empty. The length of insertion of the dielectric rod would be adjusted to tune the resonance to compensate for the detuning effect of samples being heated by the microwave field at $r/a = 0.6941$.

insertion of any objects into the cavity, the resonance frequency of the cavity would be higher than the nominal magnetron resonance frequency. Specifically, the radius of the cavity would be chosen, according to calculations of the resonance frequencies under various conditions, so that the insertion of the samples and the dielectric tuning object(s) would cause the resonance frequency to decrease to within the tuning range of the magnetron. The position of one of the dielectric object(s) would be adjusted to maintain the resonance frequency at or near the nominal magnetron resonance frequency.

The dielectric material used for tuning should have a high melting temperature. The permittivity of the tuning material should have a real part as large as possible to maximize the achievable frequency shift and an imaginary part as small as possible to minimize absorption of microwave energy. Quartz and highly pure alumina are examples of materials that fit these criteria. Because the magnitude of the frequency shift is proportional to the square of the electric field, the dielectric tuning objects should be placed at or near a position or positions of maximum electric field.

The figure illustrates how the technique could be applied to a cavity excited in the TEM_{020} mode. All of the modes in the TM_{0n0} family feature electric-field maxima along the *z* axis and at other radial positions that depend on the mode order (*n*). In the TEM_{020} mode, the off-*z*-axis maximum occurs at $r/a = 0.6941$, where *r* is the radial coordinate and *a* is the radius of the cylindrical cavity wall. Rods of sample material could be placed symmetrically about the *z* axis at $r/a = 0.6941$ to intercept the electric-field maximum there for maximum heating, while a dielectric rod (optionally surrounded by a narrow dielectric tube) could be placed at the *z* axis to intercept the electric-field maximum there for maximum tuning effect. The fine resonance frequency would be adjusted by adjusting the length of insertion of the rod. Alternatively, a sample could be placed at the *z* axis and tuning rods could be positioned symmetrically at $r/a = 0.6941$.

The position of the tuning rod could be adjusted automatically by use of a feedback control system. A sensor would provide an error signal that would be used to generate commands for a motor controller. The motor would move the rod in or out by an amount that would depend on the magnitude and sign of the difference between the actual and desired resonance frequencies. A control technique that could be adapted to this application was described in "Using Vibrations to Match Impedance of a Microwave Cavity" (NPO-19500), *NASA Tech Briefs*, Vol. 20, No. 10 (October 1996), page 56.

This work was done by Martin Barmatz of Caltech and Henry Jackson of ACRO Service Corp. for **NASA's Jet Propulsion Laboratory**. *Further information is contained in a TSP [see page 1].*

In accordance with Public Law 96-517, the contractor has elected to retain title to this invention. Inquiries concerning rights for its commercial use should be addressed to

Technology Reporting Office
JPL
Mail Stop 122-116
4800 Oak Grove Drive
Pasadena, CA 91109
(818) 354-2240

Refer to NPO-20409, volume and number of this NASA Tech Briefs *issue, and the page number.*

First-Generation "Space Cube" Electronic-Circuit Packaging

Modules are stacked and interconnected in three dimensions.

NASA's Jet Propulsion Laboratory, Pasadena, California

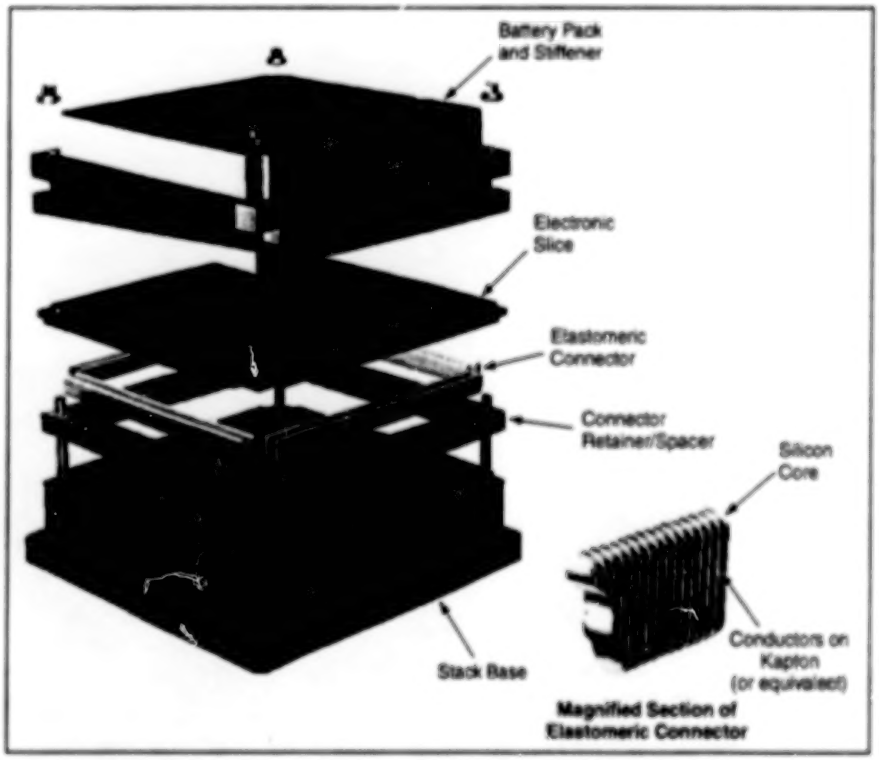

The "Space-Cube" scheme provides high packaging density, with symmetrical interconnections on all four edges of each module, and without need for interboard wiring or a back plane.

The term "space cube" denotes a scheme for three-dimensional stacking and interconnection of electronic-circuit modules. [This scheme should not be confused with a related one described in "Stackable Electronic Computer Modules and Interconnections" (NPO-19521), *NASA Tech Briefs*, Vol. 20., No. 6 (June 1996), page 33.] The figure illustrates a typical first-generation "space cube" stack. Each module in the stack is called a "circuit slice." The circuit slices are squares with edges 3.5 in. (8.89 cm) long, and with 160 electrical contacts on each edge. Electrical connections between corresponding contacts on adjacent modules are made by use of conductive strips on square elastomeric rings that are held in square retainer/spacer frames.

There is no particular limit on the thickness of a slice, on the material(s) of which it can be made, or the circuitry it can contain. For example, a circuit slice could be a multichip module; that is, it could contain multiple integrated-circuit chips on a printed-wiring board.

This work was done by Gary Bolotin and John Cardone of Caltech for **NASA's Jet Propulsion Laboratory**. *Further information is contained in a TSP [see page 1].*

In accordance with Public Law 96-517, the contractor has elected to retain title to this invention. Inquiries concerning rights for its commercial use should be addressed to

Technology Reporting Office
JPL
Mail Stop 122-116
4800 Oak Grove Drive
Pasadena, CA 91109
(818) 354-2240

Refer to NPO-20236, volume and number of this NASA Tech Briefs issue, and the page number.

Micromachined Photodiode/Bolometer Arrays

These devices could be used throughout the spectrum, from x rays through infrared.

NASA's Jet Propulsion Laboratory, Pasadena, California

Micromachined planar arrays of detectors that could operate either as photodiodes or as bolometers have been proposed for use in detecting photons in applications in which broad spectral responses are required. The availability of either of the two modes would enable operation throughout the spectrum, from x rays through infrared. Potential markets for these devices could lie in the automotive industry (infrared-image detectors for night vision), the consumer electronics industry (infrared detectors for security systems), the semiconductor industry (process-monitoring equipment), and medical electronics (x-ray detectors).

In general, bolometers enable the detection of infrared radiation, without need for cooling. The most common and most sensitive microbolometers now in use are based on thermistors made of amorphous semiconductors; the change in current through a thermally isolated microthermistor is indicative of the amount of absorbed radiation. Amorphous semiconductors are attractive as microthermistor materials because they are compatible with surface micromachining techniques that can be used to impart high degrees of thermal isolation. The disadvantages of amorphous semiconductors are low coefficients of thermal resistance and high levels of low-frequency ("1/f") noise.

In a device of the proposed type, the detectors would be single-crystal junction diodes within a micromachined structure that would provide a high degree of thermal isolation to the diodes. The diodes could be operated with forward bias to obtain the bolometric mode — usually best for detecting infrared radiation. Alternatively, the diodes could be operated with reverse bias to make them respond similarly to common photodiodes.

With respect to the functionalities of photodiodes and microthermistors, the single-crystal semiconductor materials that would be used in the proposed devices offer two important advantages over amorphous and polycrystalline semiconductors; namely, lower leakage currents and higher coefficients of thermal resistance. Exceptional thermal isolation and low thermal mass of detectors could be obtained by fabricating an array of detectors on one chip and its readout circuitry on another chip, then mating the two chips by use of hybridization techniques. For example, the detector array could be fabricated on a silicon-on-insulator chip by use of standard patterning and doping techniques, while the readout circuitry could be fabricated by standard complementary metal oxide/semiconductor processes. In the fabrication of the detector array, the thermal isolation of the detectors would be maximized and their thermal mass minimized by using surface micromachining techniques to remove most of the detector-supporting layer. The detector and readout chips could then be joined to each other by a standard technique of bonding via indium bumps on electrical-contact pads.

The sensitivity of a device of this type in the bolometric mode could be adjusted by varying the forward bias. By appropriate weighting of image data acquired in both bias modes, it should be possible to separate an image into visible and infrared parts. Depending on the selected bias, operating temperature, and spectrum of interest, a device of the proposed type may offer performance rivalling that of a quantum-well infrared photodetector (QWIP), but with a capability of operation over a wavelength range much broader than that of a QWIP. The performances of these devices may even approach theoretical limits for both thermal infrared sensors and photodiodes.

This work was done by Mark Wadsworth, Marc Foote, and Robert Beye of Caltech for **NASA's Jet Propulsion Laboratory**. *Further information is contained in a TSP [see page 1].*

In accordance with Public Law 96-517, the contractor has elected to retain title to this invention. Inquiries concerning rights for its commercial use should be addressed to

Technology Reporting Office
JPL
Mail Stop 122-116
4800 Oak Grove Drive
Pasadena, CA 91109
(818) 354-2240

Refer to NPO-20386, volume and number of this NASA Tech Briefs issue, and the page number.

BLANK PAGE

Electronic Systems

Hardware, Techniques, and Processes

15 Compact Bit-Serial VLSI Neuroprocessor for Automotive Use
15 Laser-Based Instrument Measures Vibration at a Single Point
16 Multiple-Beam Transmission for Optical Communication
17 Software for Automated Retesting of Electrical Connections

BLANK PAGE

Compact Bit-Serial VLSI Neuroprocessor for Automotive Use

Efficient utilization of hardware makes for compactness.

NASA's Jet Propulsion Laboratory, Pasadena, California

An application-specific integrated circuit (ASIC) has been developed as a prototype of neuroprocessors for real-time diagnosis and control of automotive engines. The application of this ASIC was previously reported in "Neuroprocessor for Detecting Misfire in an Automotive Engine" (NPO-20044) *NASA Tech Briefs*, Vol. 21, No. 12 (December 1997), page 60. The neuroprocessor is configured as a recurrent neural network, which differs from a conventional feedforward neural network in that the inputs to some of the neurons can include feedback signals in the form of time-lagged, weighted outputs from other neurons. Thus, the neuroprocessor responds not only to current inputs but also to the recent history of inputs.

As was previously reported, the neuroprocessor ASIC is implemented in high-speed complementary metal oxide/semiconductor (CMOS) very-large-scale integrated (VLSI) circuitry with a bit-serial architecture. By employing bit-serial techniques, this architecture makes for compactness and cost-effectiveness because (1) it entails fewer interconnections and less hardware than does bit-parallel architecture and (2) efficiency is increased through the periodic, repetitive use of the same circuitry in a time multiplexing scheme to implement successive layers in the neural network. Because the same neurons are reused in successive layers of the neural network, the total number of neurons need not exceed that of the largest layer. This architecture also affords flexibility to realize different neural-network configurations for different diagnostic or control functions; that is, multiple tasks can be performed in rapid succession, using the single neuroprocessor ASIC, by loading the synaptic-connection weights for each task at the time of that task.

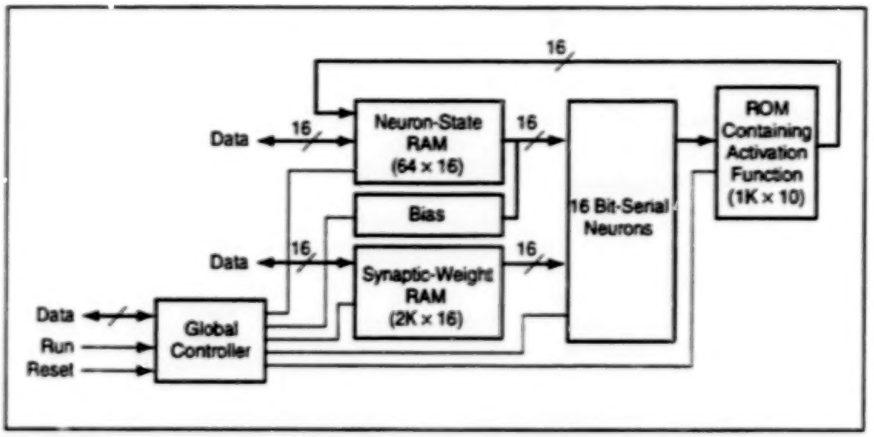

The Prototype VLSI Neuroprocessor functions as a recurrent neural network. It features a bit-serial architecture that affords compactness, cost-effectiveness, and flexibility of configuration for a variety of tasks.

The ASIC includes a module containing 16 neurons, a global controller, a read-only memory (ROM) containing a lookup table that specifies a bipolar sigmoid activation function of a neuron, a random-access memory (RAM) that serves as a register of neuron states, and a RAM containing synaptic weights (see figure). In this physical VLSI realization, each neuron receives, as inputs, synaptic weights and activation-function values from input nodes or neurons of a preceding layer in bit-serial fashion; each neuron responds by performing multiplication-and-accumulation operations that yield the value of the activation function for the given inputs.

The global controller generates the control logic and orchestrates the movement of data, as needed, to enable the rest of the ASIC to perform the required task. When a "run" command is issued, the global controller provides control signals to the 16 neurons, the RAMs, and the ROM to proceed with the desired neurocomputation. Input activations and synaptic weights are read out of the neuron-state and synaptic-weight RAMs, respectively, and sent to the neurons. Upon completion of a forward pass through the module of neurons, the global controller returns to an idle state, awaiting receipt of the next "run" command.

This work was done by Raoul Tawel of **NASA's Jet Propulsion Laboratory**. *Further information is contained in a TSP [see page 1].*

In accordance with Public Law 96-517, the contractor has elected to retain title to this invention. Inquiries concerning rights for its commercial use should be addressed to

Technology Reporting Office
JPL
Mail Stop 122-116
4800 Oak Grove Drive
Pasadena, CA 91109
(818) 354-2240

Refer to NPO-20130, volume and number of this NASA Tech Briefs *issue, and the page number.*

Laser-Based Instrument Measures Vibration at a Single Point

This compact, easy-to-use instrument measures vibrations without contact.

Dryden Flight Research Center, Edwards, California

Sponsored by a NASA Small Business Innovation Research (SBIR) Phase II contract, MetroLaser, Inc., has developed a novel, compact and low-cost laser Doppler vibrometer (LDV) under the brand name VibroMet. This LDV is a turnkey system for noncontact measurement of vibration at a single point on any vibrating structure. The system consists of two parts: a laser head and an electronic control unit (see figure) that are connected by a flexible electrical cable. Some of the notable features of the system include the following:

- Simple "point and shoot" operation for object distances from a few centimeters to 3 meters;
- Detection of signals from untreated, low-reflectivity surfaces, including black paper;
- A compact laser head that measures 2 by 3.5 by 6 in. (5.1 by 8.9 by 15.2 cm)

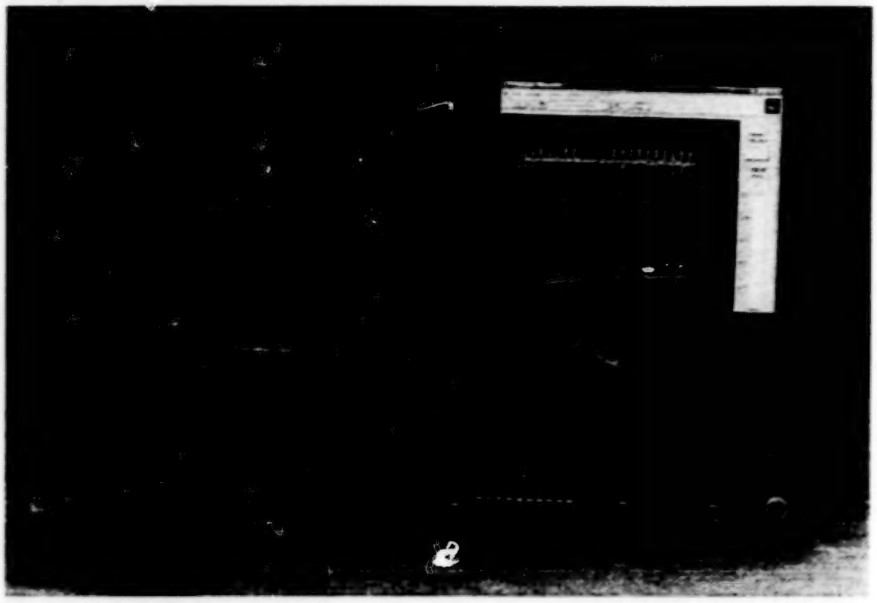

This Laser Doppler Vibrometer is a turnkey system for noncontact measurement of vibration at a single point.

and weighs less than 2 lb (<0.9 kg);
- Measurement over a wide dynamic range.

The frequency and velocity ranges of the standard VibroMet are 5 Hz to 80 kHz (at 3 dB) and 10 μm/s to 0.1 m/s, respectively. The detection ranges are expected to increase to the intervals from 2 Hz to 2 MHz and 80 μm/s to 1 m/s, respectively, in the next generation of this system.

The laser head is based on a novel configuration (patent pending) in which a diode laser and an acousto-optic modulator are the only optical elements (there are no mirrors or beam splitters). This simple optical configuration results in a robust instrument that is easy to align and straightforward to manufacture. The laser head contains all the electronic circuitry for amplification and demodulation of the Doppler vibration signal. The electronic control unit includes dc power supplies, a radio-frequency driver, a signal-strength display, and selectable signal-conditioning circuits for use as antialiasing filters.

This system can be used in many applications; examples include testing of prototypes, monitoring the health of machinery, and quality control on assembly lines. Recently, MetroLaser collaborated with the Department of Civil and Environmental Engineering of the University of California at Irvine in performing a series of experiments to explore the utility of an LDV in detection of earthquake-induced damage. The VibroMet was used to measure the natural vibrational frequencies of concrete structures that are representative of highway bridge supports. The results of the experiments conclusively demonstrated that this system can accurately measure damage induced by simulated earthquakes, which may not be detectable by visual inspection. The results of the experiments also demonstrated that natural frequencies in concrete structures can be measured by use of random excitations, such as those from vehicular-traffic vibrations or wind. Therefore, monitoring of highway bridges for damage induced by earthquakes can be accomplished quickly and without interruption of service by use of this system.

A survey by means of this system is being planned for 70 new bridges in the soon-to-be-opened Eastern Corridor Toll Road in Orange County, California. Tracking the degradation of the bridge supports over time and especially after earthquakes will both validate this system for widespread use and provide safety engineers with valuable information.

In addition to having expanded measurement ranges as mentioned above, the next generation of this system will be more compact. It is envisioned that the system will eventually be powered by batteries and the size of the laser head will be reduced to that of a pen.

This work was done by De Yu Zang, James Millerd, David Rosenthal, Eric Johnson, and Cecil Hess of MetroLaser, Inc., and Matt Tonge, an independent consultant, under an SBIR contract monitored by **Dryden Flight Research Center**.

In accordance with Public Law 96-517, the contractor has elected to retain title to this invention. Inquiries concerning rights for its commercial use should be addressed to

MetroLaser, Inc.
18010 Skypark Circle, #100
Irvine, CA 92614-6428
(949) 553-0688

Refer to DRC 098-067, volume and number of this NASA Tech Briefs *issue, and the page number.*

Multiple-Beam Transmission for Optical Communication

Superposition of mutually incoherent beams would reduce deleterious effects of atmospheric turbulence.

NASA's Jet Propulsion Laboratory, Pasadena, California

Multiple-beam transmission has been proposed to reduce the deleterious effects of atmospheric turbulence on free-space laser communications — especially on uplinks from ground stations to Earth-orbiting satellites. The deleterious effects in question are signal fades and surges associated with scintillation, beam broadening, and beam wander. These effects are caused by amplitude and phase fluctuations that, in turn, are caused by turbulence-induced spatial and temporal fluctuations in the index of refraction of air.

The basic principle of the present multiple-beam-transmission concept is one of incoherent superposition. The beam from the transmitting laser would be split into two or more beams, the optical path lengths of which would differ from each other by more than the laser coherence length. The beams would be transmitted to the receiver from points separated laterally by more than the optical coherence length of the turbulence cells in the atmosphere (for a wavelength of 0.5 μm, this length is about 10 cm). The overlap of the beams in the far field would therefore be characterized by temporal and spatial incoherence among the beams, with consequent stochastic smoothing that would reduce the magnitudes of fades and surges in the signal arriving at the receiver.

The concept was tested in experi-

ments on optical communication between a station at the Table Mountain Facility near NASA's Jet Propulsion Laboratory and a laser-communication apparatus aboard the Japanese ETS-VI satellite. In these experiments, the laser beam from the transmitter on the ground was split, variously, into two or four beams that were directed up to the satellite. Once a signal-tracking loop in the satellite was activated, the laser transmitter aboard the satellite transmitted a downlink signal to the ground station. In spite of some difficulty in deconvolving atmospheric effects from pointing errors and spacecraft vibration, analysis of data from the experiments revealed significant improvements in uplink reception with multiple uplink beams. Downlink signal fluctuations were attributed to pointing jitter, suggesting the need for highly accurate pointing to establish a stable communication link.

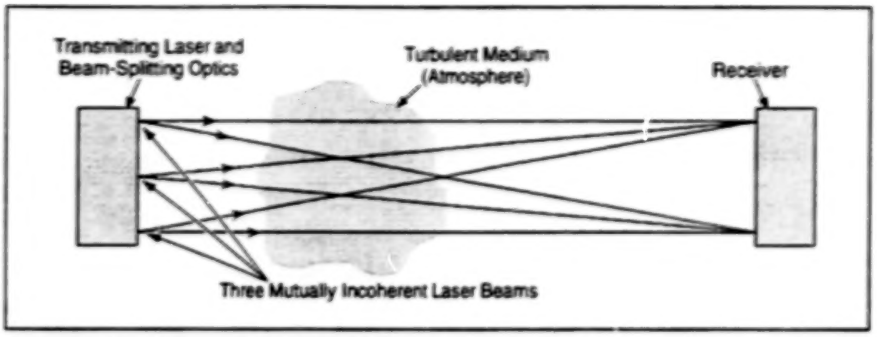

Overlapping of Mutually Incoherent Beams in the far-field can be utilized to reduce the magnitudes of signal fades and surges at the receiver.

This work was done by James Lesh and Keith Wilson of Caltech for **NASA's Jet Propulsion Laboratory**. *Further information is contained in a TSP [see page 1].*

In accordance with Public Law 96-517, the contractor has elected to retain title to this invention. Inquiries concerning rights for its commercial use should be addressed to

Technology Reporting Office
JPL
Mail Stop 122-116
4800 Oak Grove Drive
Pasadena, CA 91109
(818) 354-2240

Refer to NPO-20384, volume and number of this NASA Tech Briefs *issue, and the page number.*

Software for Automated Retesting of Electrical Connections

The Shuttle Connector Analysis Network Automated Electrical Retest Operations (SCAN/AERO) computer program assists in the tracking, management, and automation of the retesting of electrical connectors on the space shuttle orbiters. Among other things, SCAN/AERO analyzes test data to determine the statuses of connectors and of equipment affected by them. One analysis function is identification of measurements that are outside acceptable limits for affected equipment subsystems that are not listed explicitly as being disconnected at test time. Another such function is identification of current configurations of hazardous systems that are required to be maintained in predefined configurations. A graphical user interface enables the user to select an orbiter and/or an orbiter system of interest, choose a display of current configurations, request status information, or generate an engineering report. The engineering reports generated by SCAN/AERO are meant to serve as accurate and timely retest documentation and to be distributed daily (electronically and, optionally, in printed form) to affected personnel. Concepts forged from the pioneering work of the SCAN/AERO project are being incorporated into the Checkout and Launch Control System (CLCS) that is presently under development by NASA at the Kennedy Space Center. John Wilkinson is a System Software Architect for CLCS.

This work was done by Robert D. Giffen and John Wilkinson formerly of Lockheed Martin for **Kennedy Space Center**. *Further information is contained in a TSP [see page 1].*

Inquiries concerning rights for the commercial use of this invention should be addressed to the Technology Programs and Commercialization Office, Kennedy Space Center, (407) 867-6373. Refer to KSC-11985.

BLANK PAGE

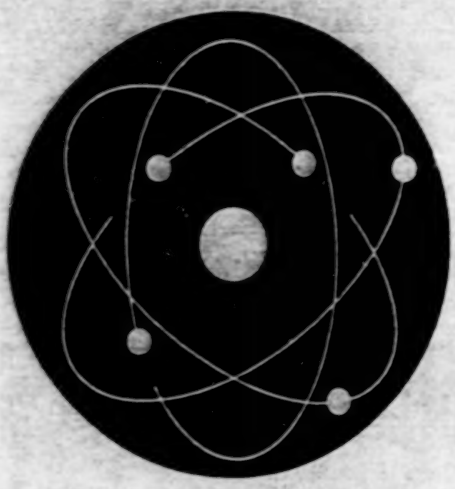

Physical Sciences

Hardware, Techniques, and Processes

21 Illumination Device for Inspecting Window Surfaces
22 Measuring Temperature of Glass by Multiwavelength Pyrometry
23 Noncontact Measurement of Resistivity of Molten Material
23 Noncontact Measurement of Surface Tension of Molten Material

BLANK PAGE

Illumination Device for Inspecting Window Surfaces

Small imperfections and dirt appear bright against a dark background.

John F. Kennedy Space Center, Florida

A special-purpose fiber-optic illumination device can be attached temporarily to a window to help an inspector examine window surfaces for scratches, pits, small-scale roughness, and dirt. This device was developed to replace an older fiber-optic illumination device that provided intense illumination to an area not much larger than the cross section of the fiber-optic light guide, had to be scanned manually over the entire window surface to complete an inspection, and often caused bright light to be reflected directly into the inspector's eyes during maneuvers ancillary to scanning. The present device illuminates a much larger area, does not shine bright light into the inspector's eyes, and leaves the inspector's hands free.

The basic illumination strategy is to launch the light into the window at an angle for which the light is totally internally reflected at smooth, flat, parallel window surfaces. Because of the total internal reflection, such surfaces appear dark when viewed from outside the window. However, surface imperfections scatter incident light, so that they appear bright when viewed from outside the window. Thus, small surface imperfections in a large area can readily be identified because they appear bright against a dark background.

The unique aspect of the present device lies in a fixture that aligns the output end of the fiber-optic light guide at the required angle and couples the light into the window (see figure). A transparent acrylic block holds the light guide at an angle of about 60° from the perpendicular to the surface of the window. The light emerges from the end of the light guide and travels through the block, through a thin interfacial layer of clear material, and into the window.

The interfacial layer can be made of clear rubber attached to the acrylic block by a clear glue. Alternatively, a liquid (e.g., water, an alcohol, an oil, or a glycerine compound) can be used as the interfacial material. In either case, it is necessary that the interfacial material fill the entire gap between the window and the block and have an index of refraction approximately equal to the indices of refraction of the acrylic and window materials, to suppress reflections at the window/block interface.

The block is mounted in a frame that can be attached to the window by use of suction cups. The depth of mounting within the frame can be adjusted so that when the suction cups are pressed against the window, the clear rubber sheet is also pressed tightly against the window.

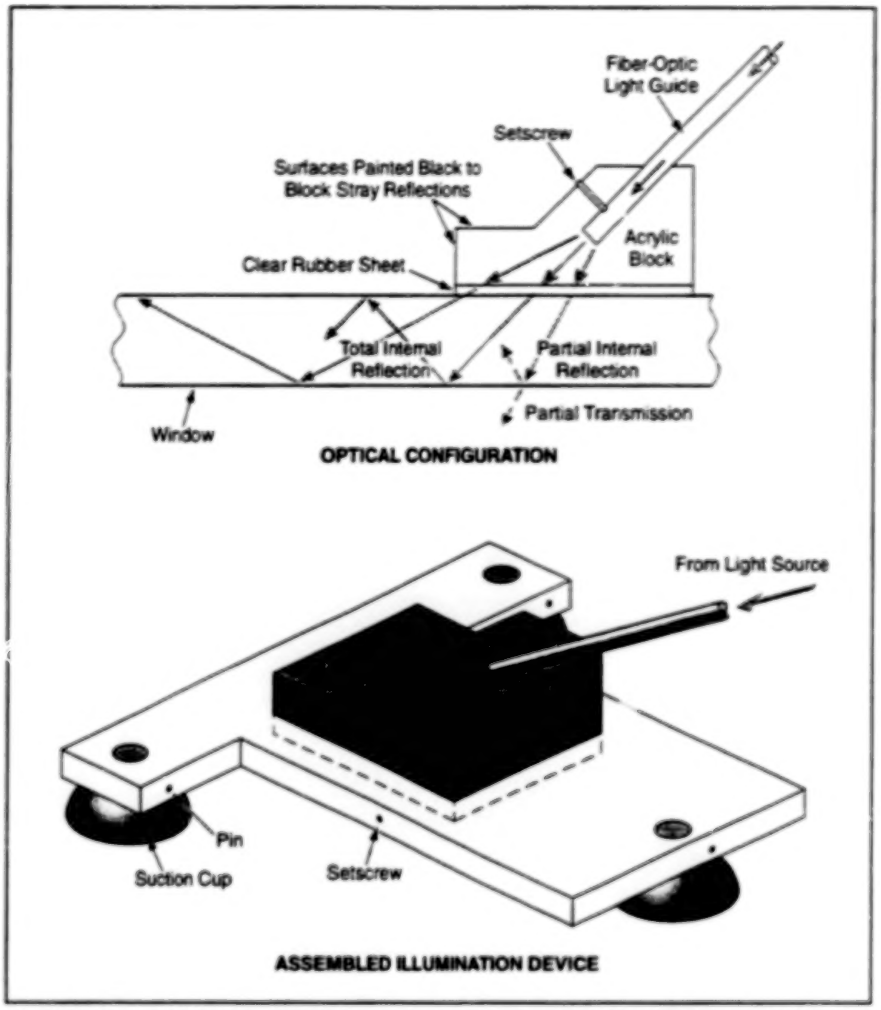

Light Is Launched Into the Window, predominantly at angles within the range of total internal reflection. The window surface as viewed from the outside therefore appears dark, except where scattering of light from surface imperfections disrupts total internal reflection, making the imperfections appear bright.

As an unavoidable consequence of the fan-out of light from the end of the fiber-optic light guide, some of this light travels at angles that are not within the range for total internal reflection. This portion of the light is partially reflected and partially transmitted at the window surface. In principle, one could incorporate a lens to reduce the fan-out, but in a typical case, the small increase in performance would not be worth the added complexity.

Because of small differences among the indices of refraction of the block, window, clear rubber, and glue, a small portion of the incident light is reflected from the interfacial region. This reflection could distract the inspector. Therefore, the exposed optical surfaces of the acrylic block are painted black to obscure the interfacial region from view.

This work was done by Barry Braden of **Kennedy Space Center**, *Robert C. Youngquist and Robert B. Cox formerly of I-NET, Inc., and Charles R. Floyd of United Space Alliance. Further information is contained in a TSP [see page 1].*

Inquiries concerning rights for the commercial use of this invention should be addressed to the Technology Programs and Commercialization Office, Kennedy Space Center, (407) 867-6373. Refer to KSC-11966.

Measuring Temperature of Glass by Multiwavelength Pyrometry

Surface and bulk temperatures are estimated from long- and short-wavelength readings, respectively.

Lewis Research Center, Cleveland, Ohio

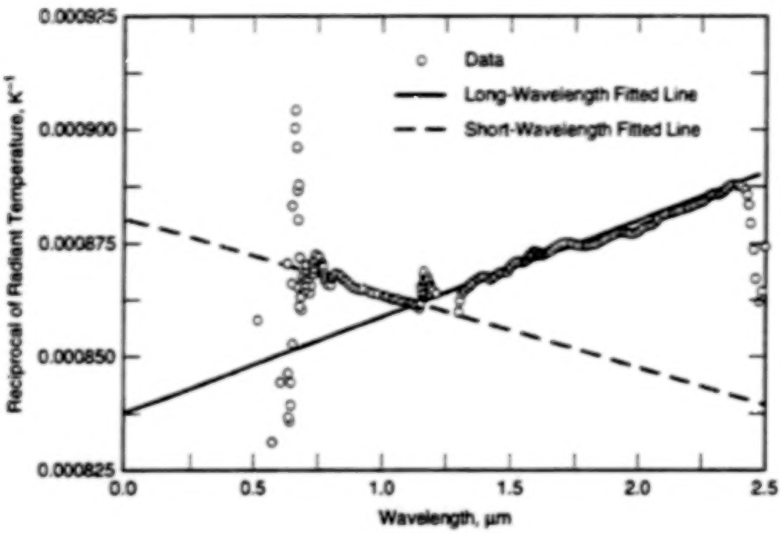

Readings of a Multiwavelength Pyrometer Were Transformed according to the equations in the text and the results plotted versus wavelength. The zero-wavelength intercepts for the long- and short-wavelength cases are the reciprocals of surface and subsurface radiant temperature, respectively.

A multiwavelength pyrometric technique estimates the surface and bulk (subsurface) temperatures of a hot glass. The multiwavelength pyrometer for which the technique was developed comprises a spectrometer plus a computer. The spectrometer can be operated in any of three wavelength ranges: 0.5 to 2.5, 0.6 to 4.5, or 2 to 14.5 μm; the range for a given measurement is generally selected according to the anticipated approximate temperature to be measured. The computer controls the spectrometer to acquire a spectrum, then analyzes the spectral data to determine the temperature.

The present technique pertains to the processing of the spectral data. Like other, related multiwavelength pyrometric techniques described in *NASA Tech Briefs* in recent years, the present technique is based partly on a modified version of Planck's radiation law. It is also based on an a distinct spectral characteristic of a typical glass; namely, that it is (1) opaque in the long-wavelength region and (2) semitransparent in the short-wavelength region of the infrared and adjacent visible spectrum to which the multiwavelength pyrometer is sensitive.

In the long-wavelength region, the radiation is emitted from the opaque surface. Planck's radiation law can be algebraically manipulated into the following equation, which is particularly useful for analyzing the spectral data:

$$\left[\frac{\ln\left(\frac{c_1}{\lambda^5}\frac{1}{L_\lambda}\right)}{c_2/\lambda}\right] - \frac{\ln\left[1-\exp\left(-\frac{c_2}{\lambda T}\right)\right]}{c_2/\lambda} = \frac{1}{T} - \frac{\lambda}{c_2}\ln(\varepsilon_\lambda \tau_\lambda)$$

where λ is the wavelength; c_1 and c_2 are constants in Planck's radiation law; L_λ is the spectral intensity at wavelength λ; ε_λ is the emissivity of the surface at wavelength λ; and τ_λ is the transmissivity, at wavelength λ, of the optical medium through which the spectrometer views the surface.

It would be convenient, for purposes of analysis, if $\varepsilon_\lambda \tau_\lambda$ turned out to be independent of wavelength. The degree to which this is true must be determined by examining the spectral data and the accuracy of the resulting interpretation. If it is true, then a plot of the left side of the equation vs. wavelength becomes a straight line with an intercept at $1/T$ — the reciprocal of the unknown temperature that one seeks to determine. For this reason, the reciprocal of the left side of the equation is often called the "radiant temperature."

In the short-wavelength region, the observed radiation originates from inside the semitransparent material. In general, there is a temperature profile $T(x)$, where x is the depth into the material. It is assumed that the spectrum of the radiation reaching the spectrometer is that of a grey body of characteristic temperature T_i, which is the bulk temperature that one seeks to determine. In this case, assuming that the wavelength is short enough to make $c_2/\lambda T >> 1$, the appropriately modified version of Planck's radiation law leads to the following equation for the reciprocal of a radiant temperature, in a form similar to that of the equation above:

$$\frac{\ln\left(\frac{c_1}{\lambda^5}\frac{1}{L_\lambda}\right)}{c_2/\lambda} = \frac{1}{T} - \frac{\lambda}{c_2}\ln\left[I(T_i,\lambda)\right]$$

where

$$I(T_i,\lambda) = \int_0^D (1-R)a\exp\left[-ax + \frac{c_2}{\lambda}\left(\frac{1}{T_i} - \frac{1}{T(x)}\right)\right]dx$$

R is the fraction of radiation reflected back into the glass at the surface and a is the absorption coefficient of the glass.

Following reasoning similar to that of the long-wavelength case, if $I(T_i,\lambda)$ were to be independent of wavelength, then a plot of the left side of the equation vs. wavelength would be a straight line with an intercept at $1/T_i$. Like the validity of the assumption of constancy of $\varepsilon_\lambda \tau_\lambda$ in the long-wavelength case, the validity of treating $I(T_i,\lambda)$ as independent of wavelength in the short-wavelength case must be determined by examination of spectral data and the resulting interpretation.

The figure is a plot of the reciprocal of radiant temperature vs. wavelength computed from multiwavelength pyrometric readings of a sample of glass heated by a propane torch. The plot clearly shows a long-wavelength region and a short-wavelength region. A straight line fit to the data from the long-wavelength region intercepts the ordinate at 0.00375 K^{-1}, corresponding to a temperature of 1,194 K; this agrees with surface temperature of 1,194 K determined by a fit to a Planck curve with an emissivity of 0.74 at all wavelengths. A straight line fit to the data from the short-wavelength region intercepts the ordinate at an ordinate that corresponds to T_i = 1,136 K. The closeness of the fit of the short-wavelength data to the straight line confirms the validity of treat-

ing $I(T,\lambda)$ as being independent of wavelength for these measurements.

This work was done by Daniel Ng of **Lewis Research Center**. *Further information is contained in a TSP [see page 1].*

Inquiries concerning rights for the commercial use of this invention should be addressed to NASA Lewis Research Center, Commercial Technology Office, Attn: Tech Brief Patent Status, Mail Stop 7–3, 21000 Brookpark Road, Cleveland, Ohio 44135. Refer to LEW-16614.

Noncontact Measurement of Resistivity of Molten Material

The basic principle of the induction motor is utilized for a different purpose.

NASA's Jet Propulsion Laboratory, Pasadena, California

It is now possible to determine the electrical resistivity of a molten sample of a pure, electrically conductive material (a metal or semiconductor), without contact between the sample or any solid object. Once the electrical resistivity has been determined, the thermal conductivity can be estimated by use of the Wiedemann-Franz-Lorenz law. (For molten materials, thermal conductivities estimated in this way are often more accurate than are thermal conductivities determined by direct measurements, because direct thermal measurements are often distorted by convection.)

It is necessary to prevent contact with the sample because typically, the molten material can become contaminated by chemical reaction with a container or other solid object. In addition, if one seeks to characterize a deeply undercooled molten material, then contact is undesirable because it can induce crystallization and thereby terminate the undercooled state.

The present method of noncontact measurement of electrical resistivity involves electrostatic levitation and noncontact heating of the sample in a vacuum chamber. The interior of the chamber is subjected to a rotating magnetic field, which exerts a torque on the sample, in essentially the same manner in which torque is generated in an induction motor. From the values of torque measured at various temperatures, one can compute the relative resistivities at those temperatures, by use of an established equation for an induction motor.

This work was done by Won-Kyu Rhim and Takehiko Ishikawa of Caltech for **NASA's Jet Propulsion Laboratory**. *Further information is contained in a TSP [see page 1].*

NPO-20369

Noncontact Measurement of Surface Tension of Molten Material

Unlike an older noncontact method, this one works even at high viscosity.

NASA's Jet Propulsion Laboratory, Pasadena, California

An improved method of noncontact measurement of the surface tension of a molten material has been developed, partly to overcome the disadvantages of contact measurement techniques as described in the preceding article, "Noncontact Measurement of Resistivity of Molten Material" (NPO-20369). This method also overcomes the primary disadvantage of an older noncontact method in which a nonrotating levitated sample is set into vibration, the frequencies of vibrational resonances are measured, and the surface tension is determined from the known relationship among the surface tension, frequencies, and other relevant quantities. The validity of the older method is limited to viscosities less than about 1 poise. The present method works over the full range of viscosities encountered in the thermal processing of metals, glasses, and metallic glasses.

Like the method of measuring resistivity described in the preceding article, the present method of measuring surface tension involves electrostatic levitation and noncontact heating of the sample in a vacuum chamber, plus the use of a rotating magnetic field to apply torque to the sample. In this case, the application of torque is metered and timed to introduce a predetermined amount of angular momentum. The magnetic field is then turned off and the sample allowed to settle into a steady state, in which it rotates as a rigid body. The shape and the frequency of rotation of the sample are measured in the steady state. Then by use of a computational model of a rotating liquid drop, the surface tension is computed for the measured shape and frequency. This method has been verified experimentally on electrostatically levitated molten drops of aluminum and tin.

This work was done by Won-Kyu Rhim and Takehiko Ishikawa of Caltech for **NASA's Jet Propulsion Laboratory**. *Further information is contained in a TSP [see page 1].*

NPO-20367

BLANK PAGE

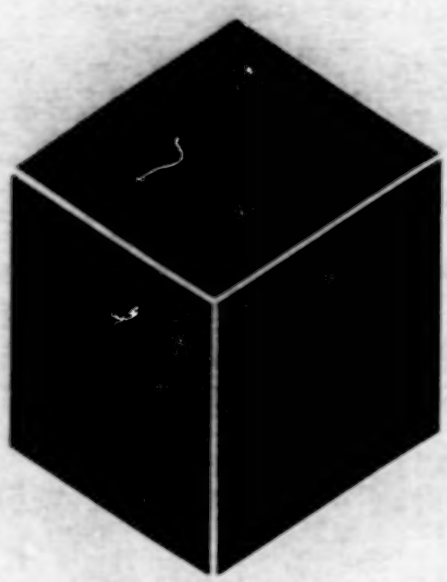

Materials

Hardware, Techniques, and Processes

27 Acid/Base Sensors Based on Poly(aromatic amine) Films
27 Improved Anode Design of Rechargeable Li-Ion Cells

Books and Reports

28 Progress in Texturing by Use of Monatomic Oxygen

BLANK PAGE

Acid/Base Sensors Based on Poly(aromatic amine) Films

Inexpensive sensors can measure concentrations in the sub-parts-per-million range.

Stennis Space Center, Mississippi

Chemiresistors containing poly(aromatic amine) films have been invented to satisfy a need for simple, inexpensive sensors for real-time measurement of parts-per-million and possibly lower concentrations of acidic and basic gases in air. These sensors could also be used to measure concentrations of acids and bases in aqueous solutions. Likely applications could include measuring concentrations of HF, HCl, HBr, and HI near incinerators in which halogenated hydrocarbons are burned; measuring concentrations of HF in and near semiconductor-processing plants; and measuring concentrations of HCl from rocket-engine exhausts. In these applications, the chemiresistors could supplant larger, heavier, more-expensive instruments that are difficult to use, do not respond in real time, and are often insufficiently sensitive.

Chemiresistors have been described in a number of previous articles in *NASA Tech Briefs*. A chemiresistor comprises a pair of metal electrodes in contact with a thin, electrically conductive polymeric film on an electrically insulating substrate. The electrical resistivity of the film increases or decreases reversibly when the film is exposed to certain chemicals. In a chemiresistor of the present type, the film is made of a poly(aromatic amine), the resistivity of which decreases upon exposure to acids in both the vapor and aqueous phases. In addition, the color of a poly(aromatic amine) varies with the acidity of its environment; thus, in principle, one could deposit a poly(aromatic amine) on the end of an optical fiber and monitor the concentration of acidic gas by measuring the optical absorption spectrum from the opposite end of the fiber.

Examples of suitable poly(aromatic amine)s include the following polymers in all of the various oxidation states in which they can exist: (1) polyaniline; (2) such derivatives of polyaniline as poly(ethylaniline), poly(butylaniline), and poly(orthotoluidine); and (3) the electroactive copolymers of polyaniline with its derivatives. Protonation (doping) or deprotonation (de-doping) of the –N= sites in these polymers leads to characteristic conductivity-versus-concentration curves that can be calibrated to obtain reliable, instantaneous readings of acid/base concentrations.

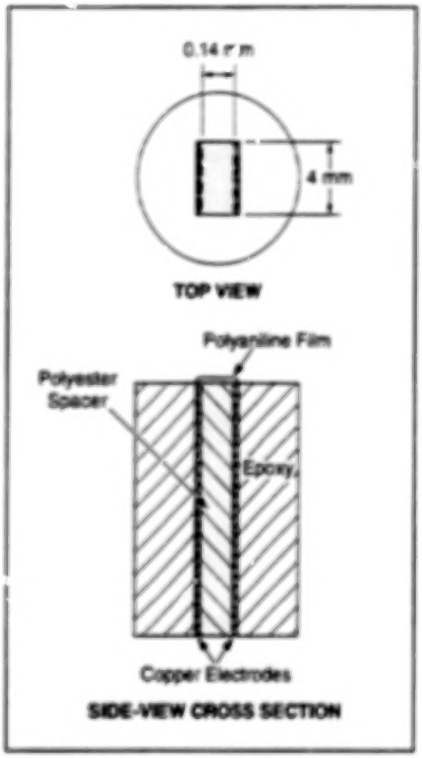

This **Prototype Sensor** was fabricated to demonstrate basic principles of the invention and is not optimized for any particular application. The sensory film was cast from a 1-percent solution of the emeraldine base form of polyaniline in N-methylpyrrolidone. The film was doped by exposure to aqueous HCl solutions at various pH levels.

A sensor of this type could be made in a variety of ways. For example, a poly(aromatic amine) film could be cast from solution on an insulating substrate to which electrodes were previously attached (see figure). Instead of a pure poly(aromatic amine), the film could consist of a poly(aromatic amine) sensory component dispersed in a nonsensory matrix of poly(methyl methacrylate), poly(vinyl chloride), or polystyrene. An array of sensors, wherein the electrode spacings, film thicknesses, and or doping levels of the sensors would differ, could be fabricated for use quantitating various acids and bases in various concentration ranges.

The doping level of a poly(aromatic amine) film can be adjusted, during fabrication, by any of a variety of chemical or electrochemical treatments. For example, a film initially in the emeraldine base (low-conductivity, blue) state can be protonated to an emeraldine salt (high-conductivity, green) state by equilibrating the film with an aqueous protonic acid. For another example, a polymeric dopant can be incorporated during polymerization or during a post-polymerization treatment.

Of the poly(aromatic amine)s, polyaniline is especially attractive, not only because it has suitable physical and chemical properties, but also because its monomer is relatively inexpensive; thus, it should be possible to manufacture relatively inexpensive (even disposable) sensors for deployment over large areas and for personal monitoring badges.

This work was done by Guang-Way Jang of Gumbs Associates, Inc., for **Stennis Space Center.**

In accordance with Public Law 96-517, the contractor has elected to retain title to this invention. Inquiries concerning rights for its commercial use should be addressed to

Ronald W. Gumbs
Gumbs Associates, Inc.
11 Harts Lane
East Brunswick, NJ 08816
(908)257-9049

Refer to SSC-00069, volume and number of this NASA Tech Briefs *issue, and the page number.*

Improved Anode Design of Rechargeable Li-Ion Cells

Proposed modifications would inhibit formation of lithium dendrites on the surface of the anode tab.

NASA's Jet Propulsion Laboratory, Pasadena, California

Several modifications of the basic design of carbon lithium-intercalating anodes with copper current collectors in rechargeable lithium-ion electrochemical cells have been proposed. These modifications are intended to prevent or at least retard the internal short-circuiting and consequent premature failure that can be caused by lithium dendrite and copper dendrite.

A rechargeable lithium-ion electrochemical cell that contains a carbon anode with

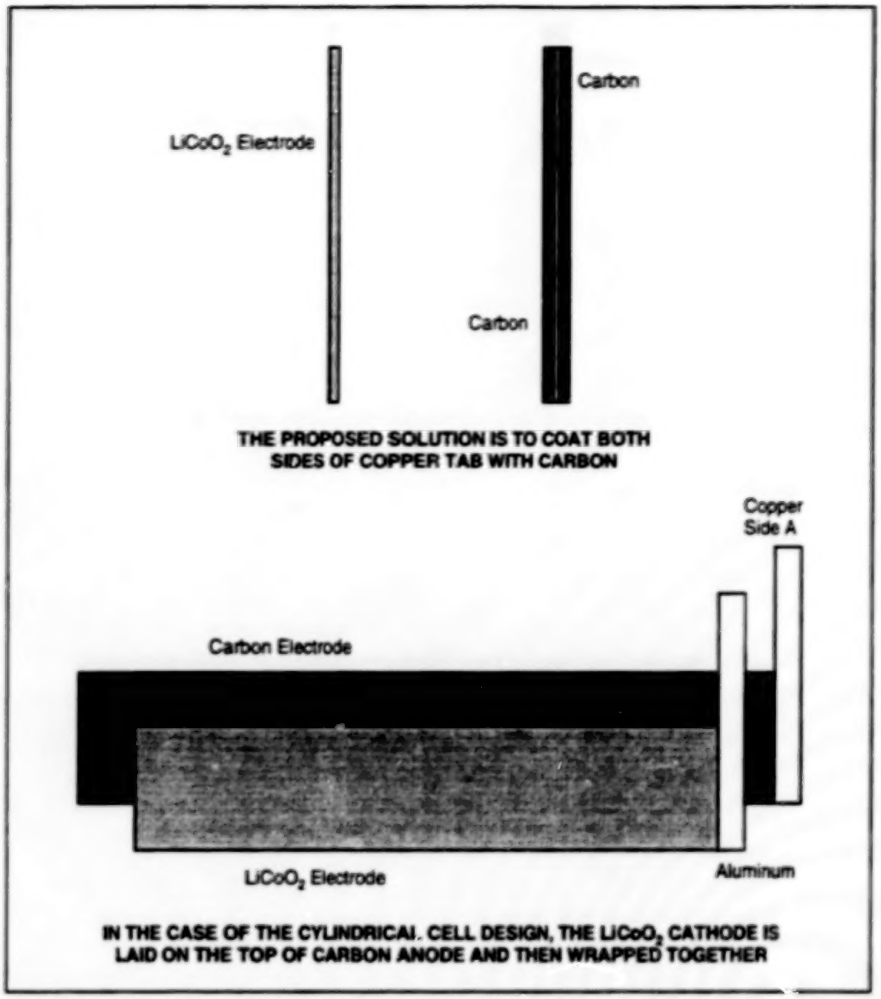
$LiCoO_2$ Electrode
Carbon
Carbon
THE PROPOSED SOLUTION IS TO COAT BOTH SIDES OF COPPER TAB WITH CARBON
Copper Side A
Carbon Electrode
$LiCoO_2$ Electrode
Aluminum
IN THE CASE OF THE CYLINDRICAL CELL DESIGN, THE $LiCoO_2$ CATHODE IS LAID ON THE TOP OF CARBON ANODE AND THEN WRAPPED TOGETHER

The **Anode Tab**, which directly faces the cathode active material, would be coated with carbon anode material to inhibit electrochemical processes that contribute to internal short-circuiting.

a copper current collector is susceptible to internal short-circuiting by either or both of two mechanisms: (1) During overcharge, lithium dendrites can grow to form conductive anode-to-cathode bridges. (2) During overdischarge, the copper current collector becomes dissolved and copper becomes redeposited elsewhere, forming a conductive anode-to-cathode bridge. In experimental cells that have become short-circuited, lithium dendrites have been found to grow on the anode tabs (which are parts of the copper current collectors), and copper deposits have been found to grow in the separators adjacent to the anode tabs.

One of the proposed modifications is to cover each anode tab, which directly faces the cathode active material, with active carbon anode material (see figure). The carbon covering would prevent direct exposure of the copper tab material to the active cathode material. The carbon covering would reduce the lithium activity at the surface of the tab sufficiently to prevent the deposition of lithium there. Another proposed modification is to orient the cathode separator pores perpendicular to the anode separator pores.

This work was done by Chen-Kuo Huang of Caltech for **NASA's Jet Propulsion Laboratory**. *Further information is contained in a TSP [see page 1].*

In accordance with Public Law 96-517, the contractor has elected to retain title to this invention. Inquiries concerning rights for its commercial use should be addressed to

Technology Reporting Office
JPL
Mail Stop 122-116
4800 Oak Grove Drive
Pasadena, CA 91109
(818) 354-2240

Refer to NPO-19966, volume and number of this NASA Tech Briefs *issue, and the page number.*

Books and Reports

Progress in Texturing by Use of Monatomic Oxygen

A report presents findings from recent research on the use of monatomic oxygen to form microscopic textures on the surfaces of polymers and extends the concept to some forms of carbon. Earlier developments in this field were described in two articles in *NASA Tech Briefs*, Vol. 20, No. 11 (November 1996): "Atomic-Oxygen Treatment To Obtain Non-Stick Polymer Surfaces" (LEW-15796) on page 44 and "Details of Atomic-Oxygen treatment of Polymer Surfaces" (LEW-15901) on page 95. In the recent research, (1) a specimen of an acrylic plastic was exposed to an atomic-oxygen plasma generated by radio-frequency dissociation of air, and (2) a specimen of pyrolytic carbon was bombarded by a directed atomic-oxygen beam (to obtain texture characterized by microscopic cones taller and more closely spaced than are those produced by the isotropic arrival of oxygen from a plasma). The specimens were examined for changes in their coefficients of static friction, water-contact angles, and optical properties (diffuse transmittance of the acrylic and thermal emittance of the pyrolytic graphite). It was concluded that atomic-oxygen texturing can be used to tailor optical properties, alter the ability to shed or retain water, improve bondability or handleability, and increase rejection of heat.

This work was done by Sharon K. Rutledge and Bruce A. Banks of **Lewis Research Center**. *To obtain a copy of the report, "Atomic Oxygen Texturing of Polymers and Carbons," see TSP's [page 1].*

Inquiries concerning rights for the commercial use of this invention should be addressed to NASA Lewis Research Center, Commercial Technology Office, Attn: Tech Brief Patent Status, Mail Stop 7-3, 21000 Brookpark Road, Cleveland, Ohio 44135. Refer to LEW-16604.

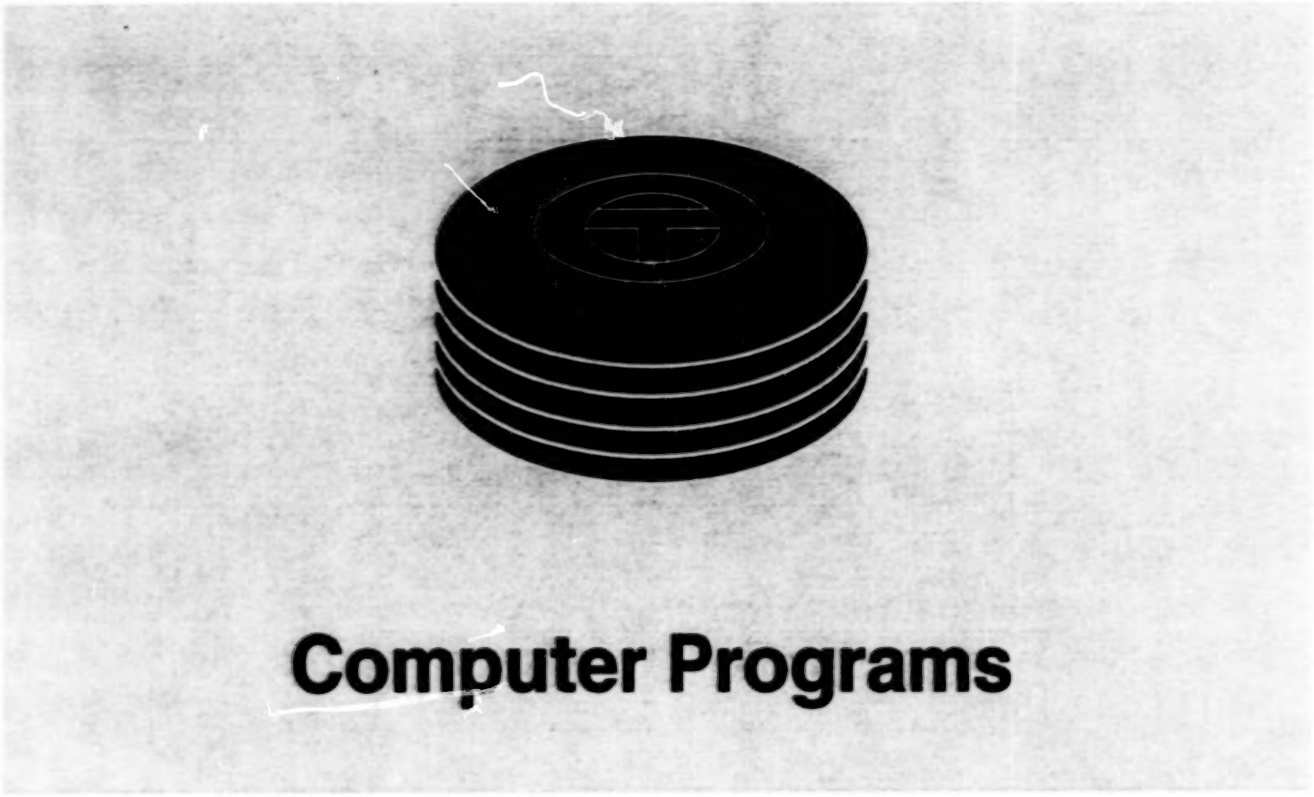

Computer Programs

Mathematics and Information Sciences

31 Program Computes Flightpaths From Point Radar Sightings

31 Program for Conceptual Design of an Attitude-Control System

BLANK PAGE

Computer Programs

These programs may be obtained from COSMIC. Please contact

COSMIC®
Computer Services Annex
University of Georgia
Athens, GA 30602
Telephone No. (404) 542-3265.

Mathematics and Information Sciences

Program Computes Flightpaths From Point Radar Sightings

A computer program estimates great-circle-arc (GARC) flightpaths of multiple aircraft, given time-tagged point locations from radar sightings of the aircraft. The problem of generating such estimates is called a "clustering" problem, and is solved in this instance by use of a neural-network clustering algorithm. Points are considered in pairs; the likelihood that any two points are on the flightpath of the same aircraft is quantified by an "association value" based on the flight dynamics of the aircraft. The program implements a Boltzmann machine, the sparse architecture of which provides for only partial satisfaction of the constraints of a cost function; this, together with a special graphical interface, serves as an aid in determining GARCs. The neural-network algorithm operates on all points simultaneously and performs a global optimization through simulated annealing; thus, it is in many instances superior to both traditional clustering algorithms that operate on points sequentially, and to other neural-network algorithms that perform local optimization. The neural network can also readily be implemented in hardware.

This work was done by John Spagnuolo, Jr., of Caltech for **NASA's Jet Propulsion Laboratory**. *Further information is contained in a TSP [see page 1].*
NPO-20288

Program for Conceptual Design of an Attitude-Control System

A report describes the ACS Design Tool — a Macintosh- and PC-based computer program for evaluating conceptual designs of a spacecraft attitude-control system (ACS) within a computation time of about 15 minutes. Services provided by the program include computation of ACS performance and sizing of ACS equipment for 3-axis gravity-gradient- and spin-stabilized spacecraft; computation of pointing jitter; computation of star-acquisition probabilities; computations of inertial quantities; radiation-shielding computations; transformation of attitude coordinate frame; conversion of units of measure; estimation of cost of an ACS at either of two different levels of complexity and accuracy; information on project definitions and standards; and data bases on celestial bodies, thrusters, ACS equipment lists, and costs for JPL missions. Developed within the Microsoft Excel software environment, this program provides easy-to-use graphical user interfaces (GUIs), including pull-down menus, scroll/increment buttons, and general buttons. The program consists of six collections of subprograms, which are summarized in the report. The report includes examples of GUI displays for all of the subprograms.

This work was done by Kenneth Lau, Edward Swenka, G. Mark Brown, Edward Mettler, Tooraj Kia, Samuel Sirlin, David Bayard, Fred Hadaegh, Edward Wong, John Lai, and Brian Cox of Caltech for **NASA's Jet Propulsion Laboratory**. *To obtain a copy of the report, "ACS(Attitude Control Subsystem) Conceptual Design Tool (software program)," see TSP's [page 1].*
NPO-20298

BLANK PAGE

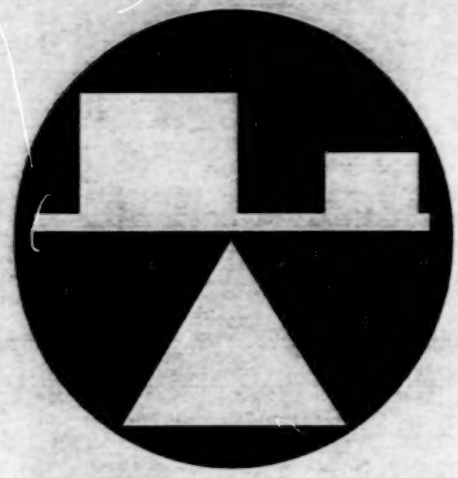

Mechanics

Hardware, Techniques, and Processes

35 Micromachined Force-Balance Anemometer
36 Estimating Attitude of a Robotic Balloon From Accelerations
37 Silicon Micromachined Accelerometer/Seismometer
37 Advanced Measurement of Angle of Attack and Sideslip

BLANK PAGE

Micromachined Force-Balance Anemometer

A micromachined force-balance accelerometer is adapted to a different use.

NASA's Jet Propulsion Laboratory, Pasadena, California

A micromachined force-balance anemometer has been developed by modifying the design of a micromachined force-balance accelerometer that responds to accelerations as small as 10^{-9} × normal Earth gravitation (about 10^{-8} m/s^2). The anemometer thus offers the advantages of the accelerometer; namely, high sensitivity, wide dynamic range, bipolar response, athermality, robustness, compactness, and low power consumption.

Both the accelerometer and anemometer versions of the design include a proof mass suspended on springs in a housing. The proof mass is in the form of two square plates, called "force plates," that are bonded together to form a single plate. The springs are thin beams (flexure springs) that lie alongside the edges of the proof mass (see figure). The springs are flexible enough to allow displacement of the proof mass along the *z* axis, but stiff enough to resist significant displacement of the proof mass along the *x* and *y* axes.

The housing includes two plates, called "quad platens," between which the proof mass is suspended on the spring flexures. In its equilibrium (non-spring-deflection) position, the proof-mass force plates lie parallel to the quad platens and about midway between them. Patterned metal coatings on the faces of the force plates and on the quad platens serve as electrodes for controlled electrostatic deflection of the proof mass and as electrodes of capacitive proximity sensors for measuring the *z* displacement of the proof mass. The quad platens are so named because each one is divided into four electrode areas. In the anemometer version, quad platens are perforated (the central half of each electrode area is removed) to allow gas to flow.

In operation, the outputs of the capacitive displacement sensors are processed through a feedback control system that applies voltages between the quad platens and force plates to keep the proof mass centered at or near the equilibrium position. These voltages serve as measures of the force with which the proof mass is deflected by acceleration (in the case of the accelerometer) or by pitot static force (in the case of the anemometer).

During handling, the proof mass can be "caged" to protect its delicate spring suspension. This is accomplished by applying an electrostatic-deflection voltage to clamp the proof mass against one of the quad platens. Submicron-thick electrically insulating surface layers prevent electrical contact between facing electrodes while allowing the interelectrode gap to become small enough to enable a small battery to generate an electric field sufficient to maintain clamping.

The overall dimensions of the micromachined anemometer are less than 2 by 2 by 0.2 cm. The dynamic range is 10^6. The frequency band of high sensitivity ranges from less than 1 to hundreds of hertz.

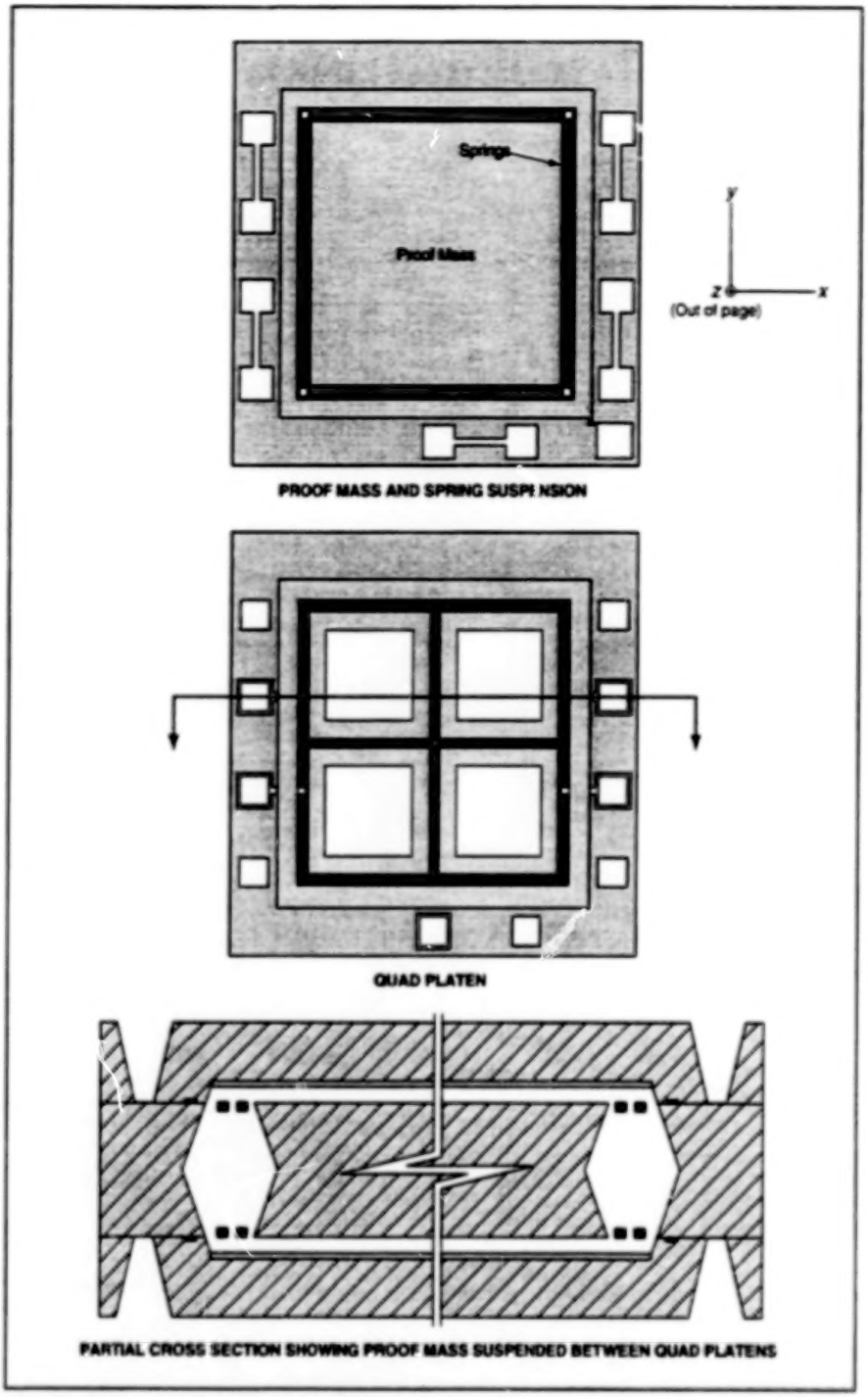

The Proof Mass Is Suspended on delicate springs. The spring suspension is not deflected during operation, and sensitivity is determined by precision of capacitance measurement.

This work was done by Frank T. Hartley and David Crisp of Caltech for **NASA's Jet Propulsion Laboratory**. *Further information is contained in a TSP [see page 1].*

NPO-20129

Estimating Attitude of a Robotic Balloon From Accelerations

The sophistication and complexity of instrumentation needed to determine attitude could be reduced.

NASA's Jet Propulsion Laboratory, Pasadena, California

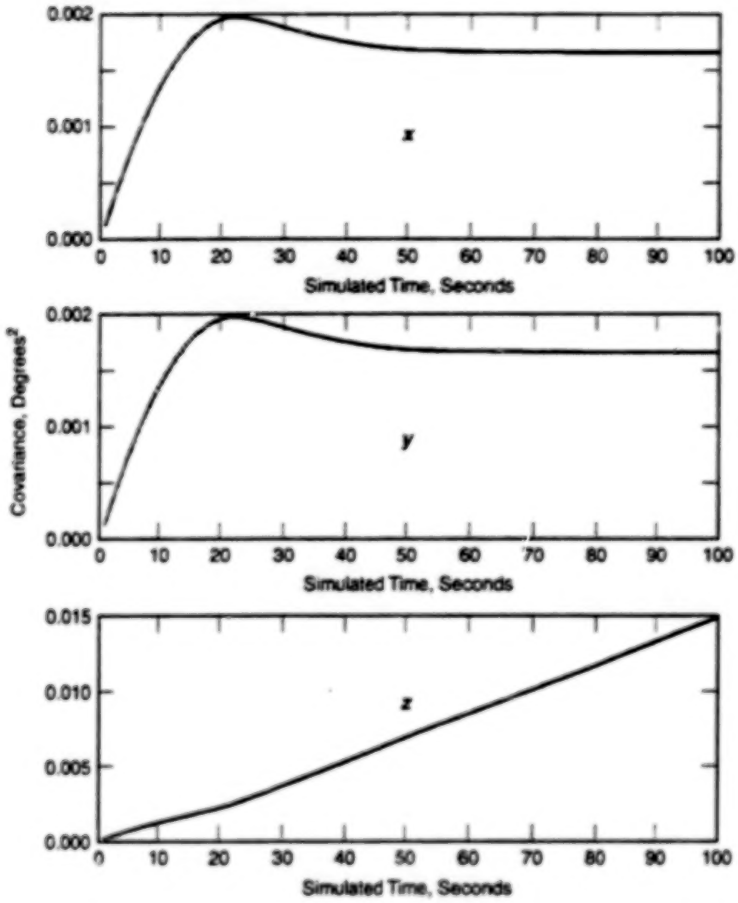

Covariances of Angular Coordinates representing rotations about the *x*, *y*, and *z* body axes evolved with time as a state-estimating mathematical model was applied in a test case. The boundedness of the *x* and *y* plots, as contrasted with the approximately linear rise of the *z* plot, demonstrates that it is possible to estimate two out of the three angular coordinates.

An improved "sensor-integrating" algorithm has been developed for use in extracting partial information on the time-varying attitude of a balloon-borne robotic instrumentation system from the outputs of accelerometers that measure accelerations along three Cartesian axes fixed in the instrument package. The partial attitude information in question comprises two coordinates, representing angles of rotation of the instrument package about two orthogonal horizontal axes. If a single additional vector measurement (e.g., the direction to the Sun) is available, then all three angular coordinates are known; that is, the attitude is fully characterized. Because the algorithm could make it unnecessary to carry a complement of conventional high-precision attitude-measuring instrumentation, it affords potential for reducing the sizes, weights, and costs of meteorological, military, planetary exploration, and other balloon-borne robotic instrumentation systems.

While the outputs of the accelerometers in the instrument package are useful for estimating changes in velocity and position, they do not directly provide attitude information. However, the outputs the accelerometers contain indirect, partial information about the attitude of the instrument package in the following sense: Each accelerometer responds to the projection, onto its axis of sensitivity, of $\mathbf{a} - \mathbf{g}$, where $\mathbf{g}$ is the gravitational acceleration and $\mathbf{a}$ is the inertial acceleration. If one knows $|\mathbf{g}|$ and can estimate $\mathbf{a}$, then one can estimate the projections of $\mathbf{g}$ onto the accelerometer axes and, from these projections, deduce the orientation of the instrument package relative to the local vertical axis.

The key to estimating $\mathbf{a}$ lies in recognizing that the motion of the balloon-borne instrumentation system is dominated by swaying like that of a pendulum with damping plus random force and torque excitations from wind gusts. For the purpose of mathematically modeling the pendulum dynamics to estimate the state of the system (the state includes the angular coordinates that one seeks), the system is approximated as a rigid body suspended below a pivot. Among the parameters of the dynamical model are the resonance frequencies of pendulum oscillations about the horizontal axes and the rates of damping of motions about all three axes. The resonance frequencies can be measured prior to flight. The rates of damping can be estimated and, even if not precise, help to ensure that, statistically, the pendulum oscillates about a vertical orientation and settles gradually to a vertical orientation when excitation is removed. The excitations from wind gusts are represented statistically, by use of first-order low-pass processes estimated from a wind power spectrum.

The dynamical model described above is converted to a nonlinear state-estimating model via an intermediate mathematical model that features a quaternion representation of attitude. The model integrates data from both accelerometers and simple gyroscopes to provide estimates of both position and attitude. The equations of the model are solved and state estimates updated by an algorithm that includes a continuous/discrete extended-Kalman-filter.

The model and algorithm were applied in a test case in which the dynamics of a balloon-borne system with representative parameters were simulated computationally. Among the results obtained in the test were covariances of the angular coordinates about the two horizontal (*x* and *y*) body axes and about the vertical (*z*) axis. As shown in the figure, the covariances for the *x* and *y* axes were found to be bounded (signifying that the angular coordinates in question can be known to within a specified accuracy), while the covariance for the *z* axis was found to increase approximately linearly with time (signifying that the estimate of the third angular coordinate deteriorates with time in the absence of further information).

This work was done by David Bayard, Robert Scheid, Donald Gennery, and Jayarao Balaram of Caltech for **NASA's Jet Propulsion Laboratory**. *Further information is contained in a TSP [see page 1].*
NPO-20315

Silicon Micromachined Accelerometer/Seismometer

A compact, silicon micromachined accelerometer is specifically designed for seismologic applications.

NASA's Jet Propulsion Laboratory, Pasadena, California

The figure illustrates a silicon micromachined accelerometer currently under development that is designed specifically for seismologic applications. The device is designed for a sensitivity of 1 ng/$Hz^{1/2}$ (where *g* denotes the Earth's gravitational acceleration, i.e., 9.81 m/s^2) and a frequency range of 0.05 to 50 Hz. Silicon micromachining allows this instrument to be much more compact, rugged, and much lighter than commercial seismometers, without sacrificing sensitivity.

Like other seismometers, the instrument is based on a proof mass suspended by springs. Electrodes are used for capacitance-sensing of the displacement and electrostatic force rebalancing of the proof mass. These electrodes, in a differential configuration as shown in the figure, also serve to cage the proof mass during deployment. Unlike conventional seismometers, however, in this implementation, the springs, proof mass, and capacitor plates are all fabricated from single crystal silicon. Silicon has a Young's modulus close to that of stainless steel and nickel and a tensile yield strength three times higher than that of stainless steel. Fabricating the device completely in silicon allows the use of well developed silicon micromachining techniques to batch fabricate the devices. It also eliminates the noise introduced by using multiple materials with differing thermal coefficients of expansion.

The accelerometer consists of two fixed capacitor plates with a proof-mass/capacitor-plate suspended between them. Selective wet chemical etching along with epitaxially grown, strain compensated, p^+ etch-stop layers are used to precisely and reproducibly form the thin silicon suspension and electrode gaps. Symmetry is used throughout the design to reduce sensitivity to off-axis accelerations and to simplify fabrication. The electrodes are fabricated by a thin chrome/gold metallization. The three plates are hermetically attached together while under vacuum, using low-temperature silicon-direct-bonding techniques. Evacuating the cavity around the proof mass reduces the squeeze film dampening between the plates, thereby raising the Q factor of the suspension. Current designs have a resonant frequency of 10 to 25 Hz and a normal capacitance gap of 5 to 10 μm.

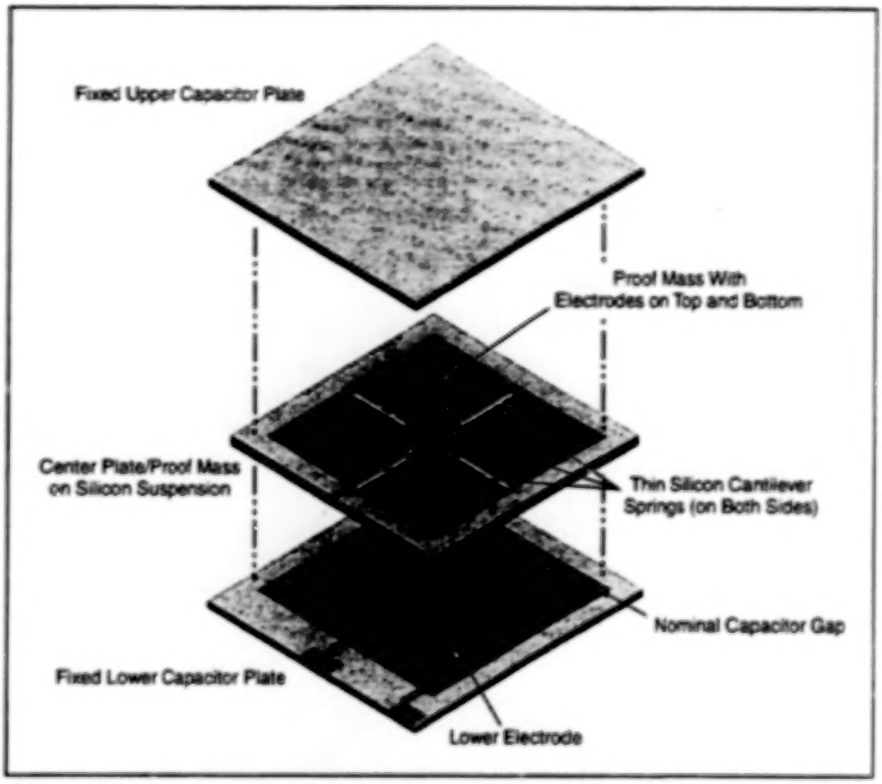
Fixed Upper Capacitor Plate
Proof Mass With Electrodes on Top and Bottom
Center Plate/Proof Mass on Silicon Suspension
Thin Silicon Cantilever Springs (on Both Sides)
Nominal Capacitor Gap
Fixed Lower Capacitor Plate
Lower Electrode

A Silicon Micromachined Accelerometer for seismologic applications is more rugged, compact, and lighter than commercial seismometers.

This work was done by Richard D. Martin and W. Thomas Pike of Caltech for **NASA's Jet Propulsion Laboratory**. *Further information is contained in a TSP [see page 1].*

In accordance with Public Law 96-517, the contractor has elected to retain title to this invention. Inquiries concerning rights for its commercial use should be addressed to

Technology Reporting Office
JPL
Mail Stop 122-116
4800 Oak Grove Drive
Pasadena, CA 91109
(818) 354-2240

Refer to NPO-19875 volume and number of this NASA Tech Briefs *issue, and the page number.*

Advanced Measurement of Angle of Attack and Sideslip

Additional airdata from advanced sensors could be used to enhance performance and safety.

Dryden Flight Research Center, Edwards, California

Nearly every military and commercial aircraft in the United States today uses pitot-static probes for accurate, repeatable airdata measurements. Recently, local angle-of-attack- and sideslip-sensing capabilities have been added to these probes to satisfy requirements for advanced aircraft with extended maneuvering envelopes. Probes made in advanced shapes to satisfy these requirements have been evaluated in wind-tunnel tests at angles of attack up to 90°, with favorable results. Flight tests of the Advanced L-probe Air Data Integration (ALADIN) program, directed toward evaluating the performances of these probes, were recently concluded at NASA Dryden Flight Research Center.

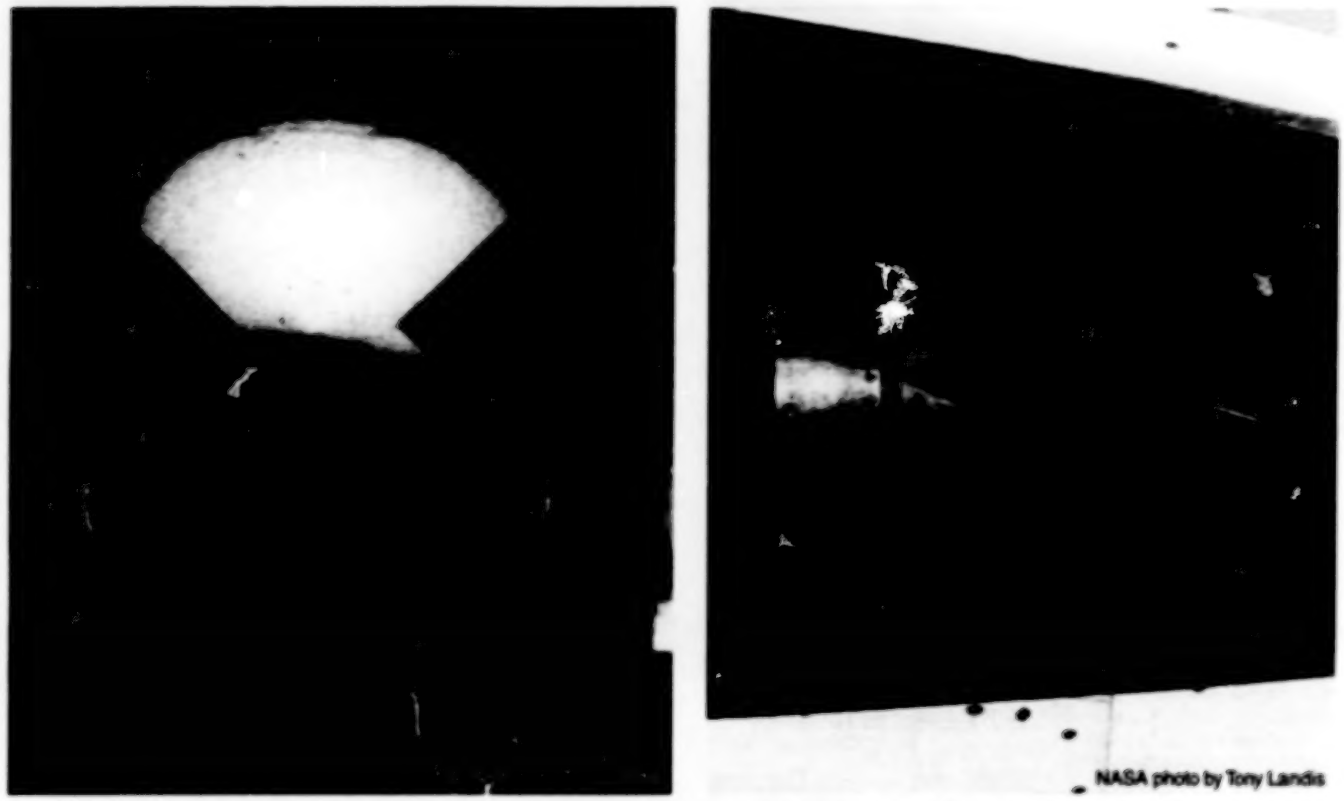

NASA photo by Tony Landis

Figure 1. **Specially Shaped Fuselage-Mounted Probes** offer advanced capabilities for sensing angles of attack and sideslip.

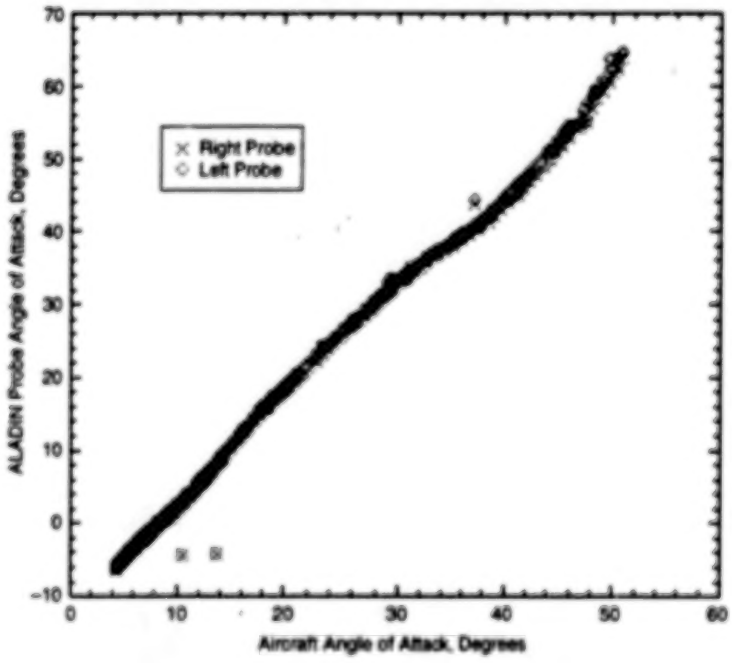

Figure 2. This is a **Flight-Test Calibration Curve** of right and left ALADIN probes at an altitude of 35,000 ft (10.7 km) and mach numbers from 0.24 to 0.74.

The ALADIN program is a cooperative effort of Boeing Phantom Works, NASA, and BFGoodrich Aircraft Sensors Division (BFG ASD). The F-18 Systems Research Aircraft (SRA), used as the flight-test platform to evaluate these probes, provides both high-angle-of-attack- and supersonic-test capabilities. The SRA is equipped with an on-board Airborne Research Tests System (ARTS) computer, is used to perform real-time airdata calculations. BFG ASD provided two multifunction L-probes and four dual-channel pressure transducers. The transducers measured pitot and static pressure directly from the probes (1 pitot and 2 static from each probe) and transmitted these values to the ARTS computer via an RS-422 interface. The ARTS computer executed an algorithm developed by BFG ASD to calculate the angles of attack and sideslip using pressure differentials from the probes. Altitude, mach number, and other airdata parameters were also calculated from these pressures. The ARTS computer transmitted the measured pressure values to the SRA data-acquisition system via a MIL-STD-1553 multiplexing bus, which was telemetered to the ground. All calculations were performed in real time and compared to reference data during flight.

ALADIN flight tests were conducted in two phases. The first phase of flights was used to evaluate the performance of the probes in different regions of the SRA flight envelope. These flights also provided data to fine-tune measured-pressure-correction tables in the ALADIN algorithm for computational fluid dynamics, wind-tunnel tests, and flight tests discrepancies. The second phase of flights involved reflying the test points from the first phase and included flight maneuvers that were similar to those of the first phase but in a different region of the flight envelope. These flights provided a set of data to check the refined calibration and to fur-

ther evaluate system performance.

The in-flight performance of the fuselage-mounted probes (see Figure 1) for the ALADIN system was found to be excellent over the typical aircraft flight envelope, with accurate tracking of altitude, mach number, and angle of attack. The BFG ASD probes and algorithm were found to be effective over a range much greater than that of the standard F-18 airdata system. Figure 2 depicts a calibration curve of probe angle of attack vs. aircraft angle of attack, as an example of the high-angle-of-attack capabilities of the ALADIN system. The ALADIN system will provide aircraft flight-control systems with more information than was previously available, thereby creating a potential to make the aircraft both safer and more capable.

Some problems identified during the flight tests are being solved with modifications to the initial algorithm. Modifications to the algorithm are being implemented by Boeing and NASA to optimize performance for angles of attack in excess of 45°. Initial evaluation of the modified algorithm developed by BFG ASD indicates that good performance can be expected even at extended angles of attack.

This work was done by Laurie Marshall of **Dryden Flight Research Center**, *Brian Barber of Boeing Phantom Works, and Roger Foster of BFGoodrich Aircraft Sensors Division. No further information is available.*

DRC-96-64

BLANK PAGE

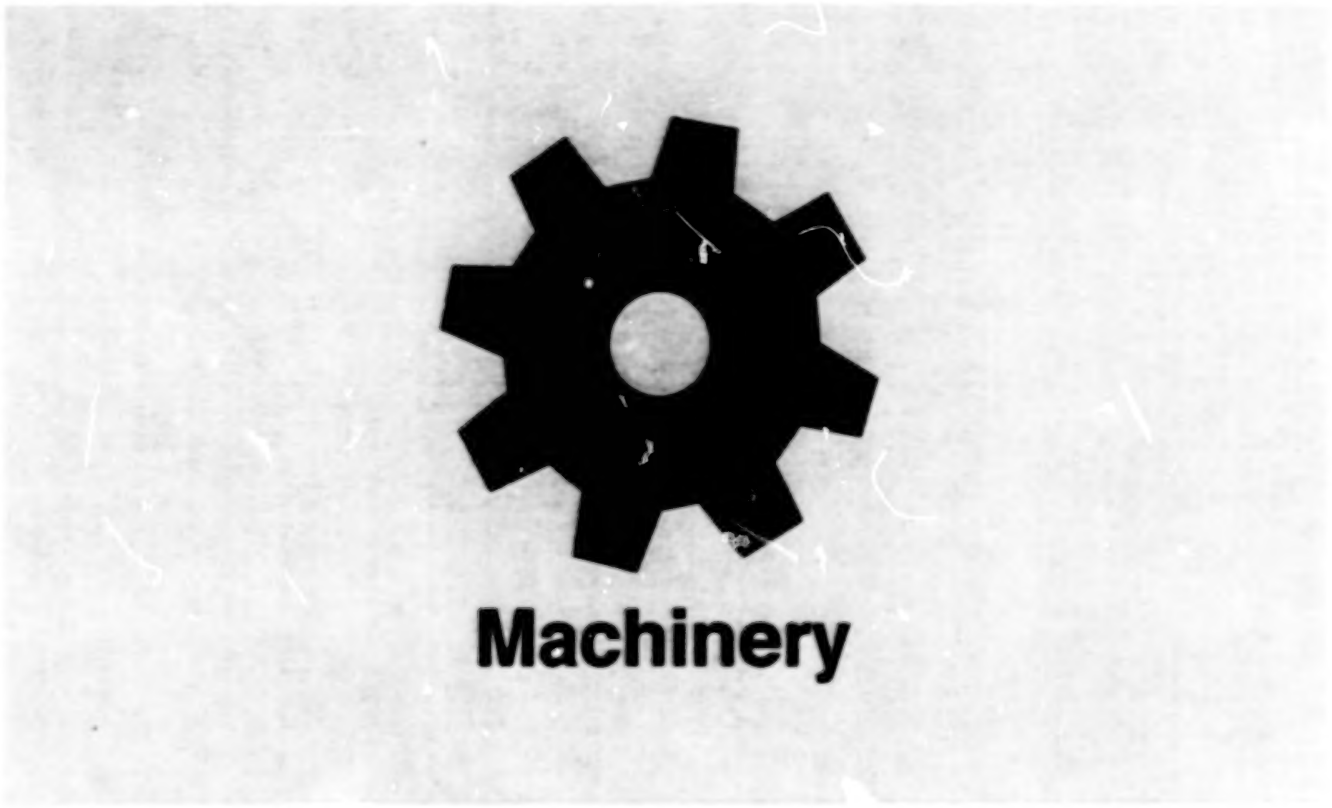

Machinery

Hardware, Techniques, and Processes

43 Swivel-Head Sampling Drill Bit

Books and Reports

44 Update on System for Robot-Assisted Microsurgery
44 Collision-Avoidance Experiments on 7-DOF Robot Arms

BLANK PAGE

Swivel-Head Sampling Drill Bit

A hard material can be sampled at depth, without need for secondary actuators.

NASA's Jet Propulsion Laboratory, Pasadena, California

A swivel-head drill bit has been invented for use in acquiring a sample of a possibly hard material at a predetermined depth. This mechanism is a simpler and thus potentially cheaper alternative to deep-coring and sampling mechanisms that contain secondary actuators to open doors and/or to drive internal sampling features. The only actuator needed to operate the swivel-head drill bit is the drill motor.

To be useful, a sampling mechanism must prevent mixing of sample material from the desired depth with material from other depths. Specifically, the present mechanism was developed subject to a requirement to limit mixing to a depth range of no more than 2 cm bracketing the desired depth. The challenge lay in satisfying this requirement without using secondary actuators.

The swivel-head drill bit includes (1) a body containing two identical sample chambers with openings at the front end capped by (2) the swivel head, which holds two cutters and can be rotated, relative to the body, to cover or uncover the openings. An integral shaft extends from behind the head through the body and is captured with a nut at the back end of the body. Small posts restrict the rotation of the head to a 90° range between the fully open and fully closed positions. The drill body and swivel head are made of MP35N alloy; the cutters are tungsten carbide inserts.

The head remains in the fully closed position as the drill bit is rotated clockwise during drilling. When the desired sampling depth has been reached, the bit is rotated counterclockwise, causing the head to swivel to the open position. The counterclockwise rotation is continued for a total of ten revolutions to move sample material into the sample chambers. Then the bit is rotated clockwise and pushed forward to swivel the head to the closed position. Finally, while rotating the bit clockwise slowly to keep the head in the closed position, the bit is withdrawn from the hole.

Swivel-head drill bits could be used to acquire subsurface samples from such diverse sources as geological sites, hazardous-waste dumps, structures, remote planets, comets, and asteroids. For example, they could be used to sample the walls and interiors of the Chernobyl nuclear reactors. In tests, the prototype swivel-head drill bit performed successfully in the acquisition of samples from the bottoms of holes in rock, plaster, and loose olivine sand.

The Swivel Turns Freely over a 90° range between two positions where it covers or does not cover, respectively, the chamber openings. The turning of the swivel head is actuated by rotation of the drill bit.

This work was done by Greg R. Gillis-Smith of Caltech for **NASA's Jet Propulsion Laboratory**. *Further information is contained in a TSP [see page 1].*
NPO-20390

Books and Reports

Update on System for Robot-Assisted Microsurgery

Two reports present updated information on a robotic system that extends the dexterity of a microsurgeon. The system was described in two articles in *NASA Tech Briefs*, Vol. 21, No. 10 (October 1997); namely, "Telerobot Control for Microsurgery" (NPO-19823), on page 46 and "Force-Feedback Device for Microsurgery" (NPO-19822), on page 86. To recapitulate, the surgeon manipulates a handle on a master robot arm, causing a slave robot arm to manipulate a surgical tool on a much finer scale, with hand tremor filtered out. The force of contact between the surgical tool and the patient's tissue is amplified and fed back to the surgeon's hand through the master robot arm. The system comprises (1) a mechanical subsystem (including motors, gears, pulleys, cables, and linkages); (2) an electronic subsystem (power amplifiers, relays, and safety circuits); (3) another electronic subsystem (servocontrol hardware and software); and (4) a high-level software subsystem. One report describes these subsystems, then describes a single-arm eye microsurgical procedure and a dual-arm microsurgical procedure that were performed to demonstrate the capabilities of the system. The report also proposes the use of the system in important secondary applications: as a simulator for training microsurgeons and as a data-collection system for evaluating the performances of surgeons in training and for research on manual dexterity.

This work was done by Curtis Boswell, Hari Das, Robert Steele, Timothy Ohm, and Edward Barlow of Caltech and Steve Charles of MicroDexterity Systems, Inc., for **NASA's Jet Propulsion Laboratory**. *To obtain a copies of the reports, "Tool actuation and force feedback on robot assisted microsurgery system" and "Robot Assisted MicroSurgery Development at JPL," see TSP's [page 1].*

In accordance with Public Law 96-517, the contractor has elected to retain title to this invention. Inquiries concerning rights for its commercial use should be addressed to

Technology Reporting Office
JPL
Mail Stop 122-116
4800 Oak Grove Drive
Pasadena, CA 91109
(818) 354-2240

Refer to NPO-20408, volume and number of this NASA Tech Briefs *issue, and the page number.*

Collision-Avoidance Experiments on 7-DOF Robot Arms

A report describes experiments on the concept described in "Real-Time Collision Avoidance for a Robot Arm" (NPO-19861), *NASA Tech Briefs*, Vol. 20, No. 12 (December 1996), page 98. Under this concept, collision-avoidance software processes data computed by model-based obstacle-detection software to generate perturbations of the trajectory of a robot arm away from the commanded trajectory whenever the commanded trajectory brings the arm within a specified distance from one or more obstacle(s). In computing the perturbation, the software strives to nullify a virtual repulsive force proportional to the incursion of the obstacle plus a virtual damping force proportional to the closing velocity of the arm and the obstacle. The experiments were performed on seven-degree-of-freedom (7-DOF) robot arms. Two of the experiments demonstrated perturbation of the position and orientation, respectively, of the end effector. In one experiment, the arm angle was perturbed to avoid an impending collision. Other experiments demonstrated avoidance of a collision between two robot arms and between different links of the same robot arm. Still another experiment demonstrated automatic countermanding of a manual teleoperation command that would have caused a robot arm to collide with a nearby structure.

This work was done by Homayoun Seraji, Bruce Bon, and Robert Steele of Caltech for **NASA's Jet Propulsion Laboratory**. *To obtain a copy of the report, "Experiments in Real-Time Collision Avoidance for Dexterous 7-DOF Arms," see TSP's [page 1].*

NPO-20336

National Aeronautics and
Space Administration

END

02\23\99